Article

TRANSPARENT PROCESS OPEN ACCESS

THE EMBO JOURNAL

Novel function of Tau in regulating the effects of external stimuli on adult hippocampal neurogenesis

Noemí Pallas-Bazarra[1,2], Jerónimo Jurado-Arjona[1,2], Marta Navarrete[1], Jose A Esteban[1], Félix Hernández[1,3], Jesús Ávila[1,2,**] & María Llorens-Martín[1,2,*]

Abstract

Tau is a microtubule-associated neuronal protein found mainly in axons. However, its presence in dendrites and dendritic spines is particularly relevant due to its involvement in synaptic plasticity and neurodegeneration. Here, we show that Tau plays a novel *in vivo* role in the morphological and synaptic maturation of newborn hippocampal granule neurons under basal conditions. Furthermore, we reveal that Tau is involved in the selective cell death of immature granule neurons caused by acute stress. Also, Tau deficiency protects newborn neurons from the stress-induced dendritic atrophy and loss of postsynaptic densities (PSDs). Strikingly, we also demonstrate that Tau regulates the increase in newborn neuron survival triggered by environmental enrichment (EE). Moreover, newborn granule neurons from Tau$^{-/-}$ mice did not show any stimulatory effect of EE on dendritic development or on PSD generation. Thus, our data demonstrate that Tau$^{-/-}$ mice show impairments in the maturation of newborn granule neurons under basal conditions and that they are insensitive to the modulation of adult hippocampal neurogenesis exerted by both stimulatory and detrimental stimuli.

Keywords adult hippocampal neurogenesis; environmental enrichment; retrovirus; stress; Tau

Subject Categories Neuroscience

DOI 10.15252/embj.201593518 | Received 18 November 2015 | Revised 1 April 2016 | Accepted 21 April 2016 | Published online 19 May 2016

The EMBO Journal (2016) 35: 1417–1436

Introduction

Tau is a neuronal microtubule-associated protein (MAP) that promotes microtubule assembly and stabilization (Weingarten *et al*, 1975). It plays key roles in the establishment of neuronal polarity and migration during embryonic development (Caceres & Kosik, 1990; Dawson *et al*, 2001; Sapir *et al*, 2012; Sayas *et al*, 2015), in axonal transport (Ballatore *et al*, 2007; Hernandez & Avila, 2010) and in intracellular trafficking (Hernandez & Avila, 2010). Under physiological conditions, Tau is located mainly in axonal microtubules (Hirokawa *et al*, 1996; Aronov *et al*, 2001), although increasing evidence supports its presence also in dendrites (Ittner *et al*, 2010) and dendritic spines (Ittner *et al*, 2010; Mondragon-Rodriguez *et al*, 2012; Kimura *et al*, 2014). The affinity of Tau to bind microtubules is finely regulated, depending mainly on the selective expression of various isoforms and post-translational modifications. Tau protein is encoded by *mapt* gene. Human *mapt* contains 16 exons, from which several Tau isoforms are generated by alternative splicing (Goedert *et al*, 1989; Andreadis *et al*, 1992). Exon 10 encodes one of the four repeat sequences that form the microtubule-binding domain. The presence or absence of exon 10 results in Tau isoforms with four (Tau4R) or three (Tau3R) repeat sequences, Tau4R showing a higher affinity to bind microtubules than Tau3R ones (Lu & Kosik, 2001; Avila *et al*, 2004). At early developmental stages, Tau3R predominates (Lu & Kosik, 2001; Avila *et al*, 2004), conferring a lower stability of the cytoskeleton and allowing the morphological differentiation and migration of developing neurons. In contrast, in the adult murine brain, Tau4R is the predominant isoform (Lu & Kosik, 2001; Avila *et al*, 2004), thereby guaranteeing the stability of the cytoskeleton required to maintain neuronal integrity. It is important to note an exception that occurs during adult hippocampal neurogenesis (AHN), when Tau3R isoforms can be found (Bullmann *et al*, 2007; Llorens-Martin *et al*, 2012).

Adult neurogenesis occurs in discrete brain regions during adulthood. Among these regions, the hippocampal dentate gyrus (DG) has attracted increasing attention due to the functional relevance of AHN, a process related to hippocampal-dependent learning and mood regulation (Sahay & Hen, 2008; Aimone *et al*, 2011). AHN encompasses the proliferation of adult neural stem

1 Centro de Biología Molecular Severo Ochoa (CSIC-UAM), Madrid, Spain
2 Centro de Investigación Biomédica en Red sobre Enfermedades Neurodegenerativas (CIBERNED, ISCIII), Madrid, Spain
3 Sciences Faculty, Autonoma University, Madrid, Spain
*Corresponding author. Tel: +34 91 196 45 92; Fax: +34 91 196 44 20; E-mail: m.llorens@csic.es
**Corresponding author. Tel: +34 196 45 64; Fax: +34 91 196 44 20; E-mail: javila@cbm.csic.es
[The copyright line of this article was changed on 17 June 2016 after original online publication.]

cells, their differentiation into mature neurons, and their incorporation into the hippocampal circuitry (Ming & Song, 2005). Furthermore, the addition of new neurons to the hippocampal circuit is regulated by numerous external factors such as physical activity, environmental enrichment (EE), and stress (Gould *et al*, 1997; Kempermann *et al*, 1997), thus conferring an outstanding degree of plasticity to the network.

By using a Tau knockout mouse model (Dawson *et al*, 2001), here we demonstrate that Tau is involved in the morphological differentiation and synaptic integration of newborn hippocampal granule neurons *in vivo*. Moreover, we report a novel function of Tau in the regulation of the negative consequences of acute stress on AHN. We also demonstrate, for the first time, that Tau regulates the stimulatory effects of EE on AHN.

Results

Tau protein is not involved in the regulation of the basal rate of adult hippocampal neurogenesis (AHN)

We first examined whether Tau protein is involved in the regulation of AHN under basal conditions. Figure 1A–D shows that the absence of Tau did not affect the number of proliferative phosphohistone 3 $(PH3)^+$ cells ($t = 0.757$; $P = 0.471$) or the number of apoptotic caspase-cleaved actin $(fractin)^+$ cells ($t = -0.771$; $P = 0.452$) in the DG. However, as proliferation and death rates are general parameters that may not reflect changes in specific cell subpopulations, we also analyzed the survival of 1-, 2-, 4-, 6-, and 8-week-old cells labeled with the thymidine analogs 5-iodo-2′-deoxyuridine (IdU) or 5-chloro-2′-deoxyuridine (CldU). Figure 1E shows the experimental design. Tau depletion did not alter cell survival at any of the ages studied (Fig 1F). Hence, we conclude that Tau protein is not involved in the regulation of newborn neuron survival rate. Figure 1G summarizes the main cell markers expressed during the sequential differentiation stages that newborn neurons go through before they become fully mature. We addressed whether Tau deficiency affects the differentiation of newborn granule neurons and their commitment to neural lineage. To explore this notion, the percentage of cells that expressed doublecortin (DCX) and neuronal nuclei (NeuN) markers was evaluated in 1-, 4-, and 8-week-old $CldU^+$ or IdU^+ newborn neurons. As expected, DCX expression decreased with time, whereas the opposite effect was observed for NeuN (Fig 1H). No differences in the expression of either of these markers were found in response to Tau deficiency. Thus, it can be concluded that Tau is not involved in newborn neuron differentiation under basal conditions. Moreover, the absence of Tau did not alter the number of Sex determining region Y-box 2 $(Sox2)^+$ ($t = -1.180$; $P = 0.261$) or brain lipid-binding protein $(BLBP)^+$ ($t = -1.015$; $P = 0.330$) neural progenitor cells. In addition, no differences in the number of DCX^+ neuroblasts ($t = -1.201$; $P = 0.253$) or in the number of $calretinin^+$ immature neurons ($t = -1.427$; $P = 0.179$) were found in $Tau^{-/-}$ mice compared to WT (Fig 1I–N). All together, these data suggest that neither is Tau involved in the regulation of AHN rate under basal conditions.

Tau protein is necessary for the dendritic maturation of newborn granule neurons

To study the role of Tau in the morphological maturation of newborn neurons, we analyzed the morphology of the dendritic tree of 4- and 8-week-old newborn granule neurons labeled with PSD95-GFP-expressing retroviruses. Figure 2A shows representative images of 4-week-old newborn granule neurons of WT and $Tau^{-/-}$ mice. In these neurons, the absence of Tau decreased the total dendritic length ($t = 4.963$; $P < 0.001$) (Fig 2B). Moreover, Sholl's analysis revealed alterations in the complexity of the dendritic tree (Fig 2C). In particular, Tau deficiency decreased dendritic branching in 100–150 μm ($t = 2.397$; $P = 0.020$), 150–200 μm ($U = 143$; $P < 0.001$), and 200–250 μm ($U = 354$; $P = 0.037$) from the cell soma. Figure 2D shows representative images of 8-week-old newborn granule neurons of WT and $Tau^{-/-}$ mice. However, at this cell age, the absence of Tau did not lead to differences in the total dendritic length ($t = -1.266$; $P = 0.210$) (Fig 2E) or in the complexity of the dendritic tree (Fig 2F).

Taken together, these results show that Tau is involved in the morphological maturation of newborn granule neurons, since its absence causes a transient alteration of the dendritic arborization of these cells.

Figure 1. Tau protein is not involved in regulating the rate of adult hippocampal neurogenesis under basal conditions.

A, B Representative image of a proliferative cell in the DG labeled with an anti-PH3 antibody (green) (A) and quantification of the number of $PH3^+$ cells in the DG of WT and $Tau^{-/-}$ mice (B) (mean ± SEM; $n = 10$ WT mice, $n = 8$ $Tau^{-/-}$ mice; Student's *t*-test).

C, D Representative image of an apoptotic cell in the DG labeled with an anti-fractin antibody (red) (C) and quantification of the number of $fractin^+$ cells in the DG of WT and $Tau^{-/-}$ mice (D) (mean ± SEM; $n = 10$ WT mice, $n = 8$ $Tau^{-/-}$ mice; Student's *t*-test).

E, F Schematic diagram of the cell survival experimental design using thymidine analogs (E) and quantification of the percentage of surviving cells in $Tau^{-/-}$ mice as compared to WT mice at each cell age (1-, 2-, 4-, 6-, and 8-week-old cells) (F) (mean ± SEM (normalized data); Student's *t*-test).

G Schematic diagram of the cell markers representative of each maturational stage during adult hippocampal neurogenesis.

H Quantification of the percentage of 1-, 4-, and 8-week-old newborn neurons that express the DCX neuroblast marker and the NeuN mature neuron marker in WT and $Tau^{-/-}$ mice (χ^2 test).

I, J Representative images of progenitor cells in the DG labeled with anti-Sox2 (red) and anti-BLBP (green) antibodies (I) and neuroblasts and immature neurons labeled with anti-DCX (red) and anti-calretinin (green) antibodies, respectively (J).

K–N Quantification of the number of $Sox2^+$ (K), $BLBP^+$ (L), DCX^+ (M), and $calretinin^+$ (N) cells in the DG of WT and $Tau^{-/-}$ mice (mean ± SEM; $n = 10$ WT mice, $n = 8$ $Tau^{-/-}$ mice; Student's *t*-test).

Data information: The number of animals used for the quantification with thymidine analogs (F, H) is indicated in (E). In representative images, cell nuclei were labeled with DAPI (blue). White scale bars, 10 μm. Red scale bars, 20 μm. GL: granular layer; SGL: subgranular layer; H: hilus. Brightness and contrast of representative confocal microscopy images shown in the figure were minimally adjusted in order to improve visualization.

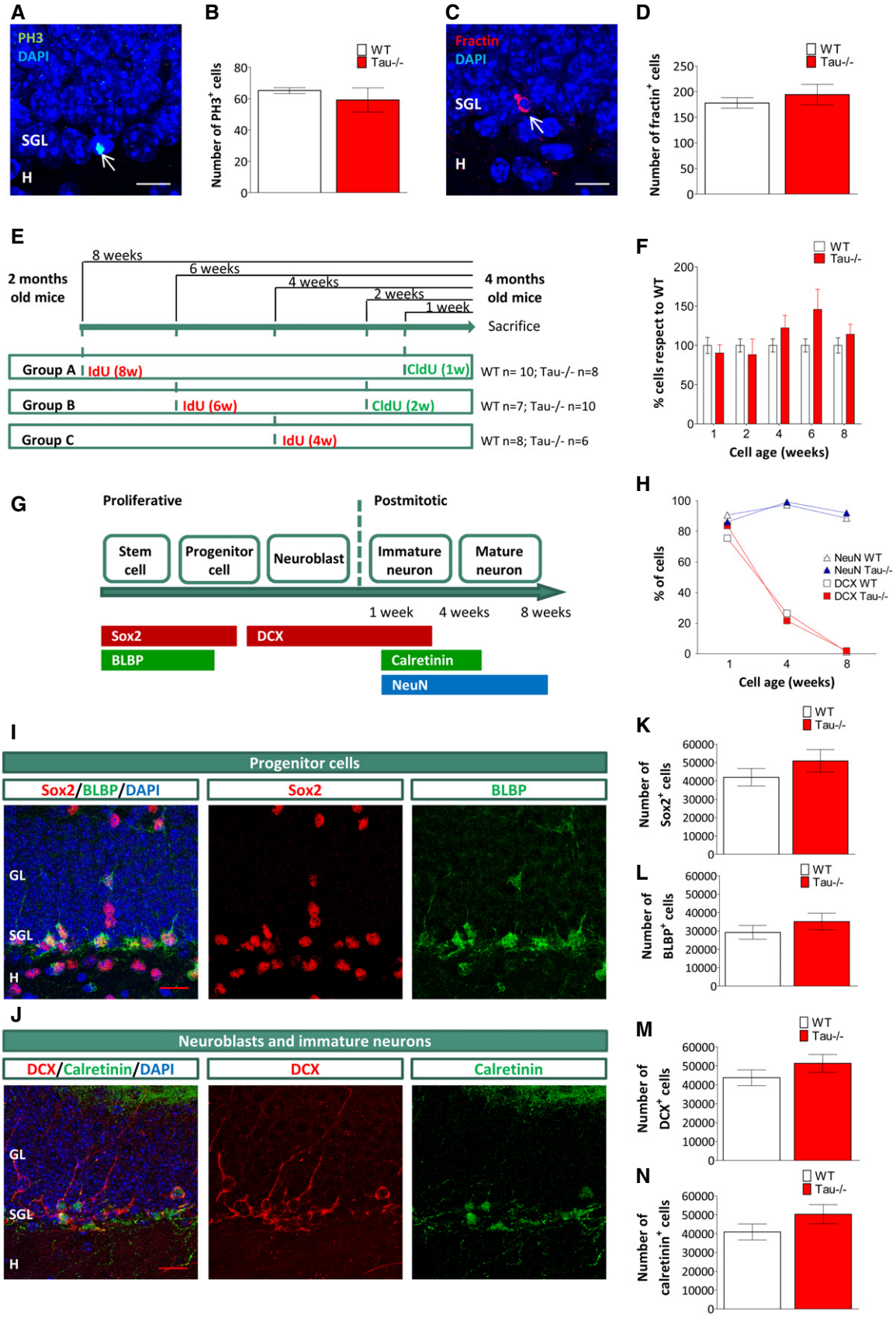

Figure 1.

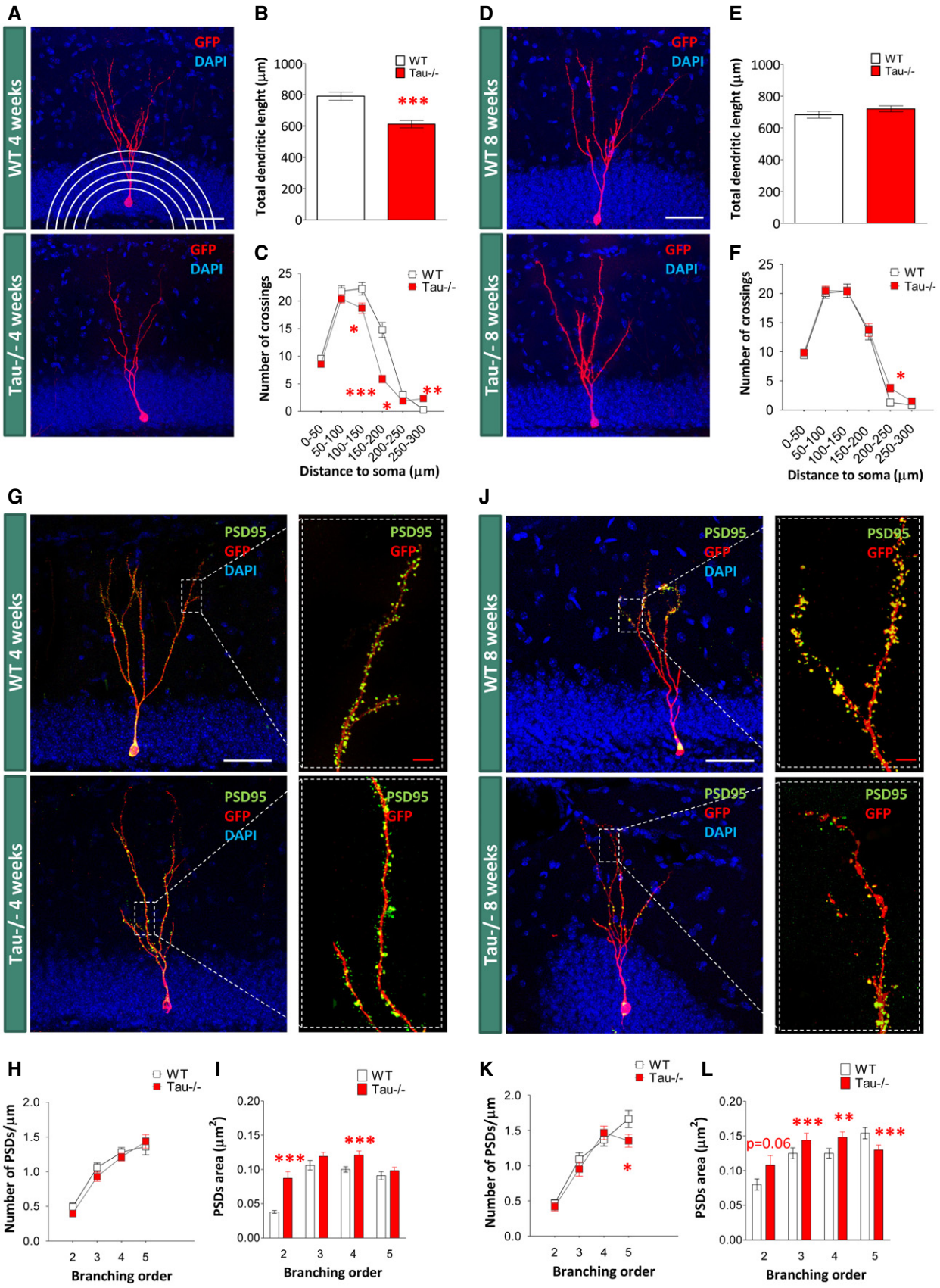

Figure 2.

Figure 2. Tau protein is necessary for the dendritic and synaptic maturation of newborn granule neurons.

A Representative images of 4-week-old newborn granule neurons of WT and Tau$^{-/-}$ mice infected by a PSD95-GFP-expressing retrovirus. A schematic representation of Sholl's analysis is shown in the WT image.

B, C Quantification of total dendritic length (B) and Sholl's analysis (C) of 4-week-old newborn granule neurons in WT and Tau$^{-/-}$ mice.

D Representative images of 8-week-old newborn granule neurons of WT and Tau$^{-/-}$ mice infected by a PSD95-GFP-expressing retrovirus.

E, F Quantification of total dendritic length (E) and Sholl's analysis (F) of 8-week-old newborn granule neurons in WT and Tau$^{-/-}$ mice.

G Representative images of 4-week-old newborn granule neurons of WT and Tau$^{-/-}$ mice infected by a PSD95-GFP-expressing retrovirus and their corresponding high-power magnifications showing PSDs (green).

H, I Quantification of the number of PSDs/μm (H) and PSD area (I) in each dendritic branching order of 4-week-old newborn granule neurons in WT and Tau$^{-/-}$ mice.

J Representative images of 8-week-old newborn granule neurons of WT and Tau$^{-/-}$ mice infected by a PSD95-GFP-expressing retrovirus and their corresponding high-power magnifications showing PSDs (green).

K, L Quantification of the number of PSDs/μm (K) and PSD area (L) in each dendritic branching order of 8-week-old newborn granule neurons in WT and Tau$^{-/-}$ mice.

Data information: In (B, C, E, F, H, I, K, L), data are presented as mean ± SEM; $n = 3$ mice per genotype; *$P < 0.05$, **$P < 0.01$, ***$P < 0.001$ (Student's t-test or Mann–Whitney U-test). In representative images, cell nuclei were labeled with DAPI (blue). White scale bars, 50 μm. Red scale bars, 5 μm. Brightness and contrast of representative confocal microscopy images shown in the figure were minimally adjusted in order to improve visualization.

Tau protein is necessary for the formation of postsynaptic densities (PSDs), dendritic spines, and mossy fiber terminals (MFTs) in granule neurons

In addition to the morphology of newborn neurons, we examined the participation of Tau in the functional maturation of these cells. Figure 2G shows representative images of 4-week-old WT and Tau$^{-/-}$ newborn granule neurons infected with PSD95-GFP-expressing retroviruses and their respective high-power magnifications, in which PSDs (afferent synapses) can be observed. No differences were found in PSD density along the dendritic tree (Fig 2H). However, the average PSD area was higher in the 2nd ($U = 56{,}105$; $P < 0.001$) and 4th ($U = 992{,}492$; $P < 0.001$) branching orders of Tau$^{-/-}$ dendrites compared to WT ones (Fig 2I). The absence of Tau in 8-week-old WT and Tau$^{-/-}$ newborn neurons (Fig 2J), fully integrated into the circuitry and infected with PSD95-GFP-expressing retroviruses, decreased the density ($t = 2.034$; $P = 0.047$) (Fig 2K) and area ($U = 1{,}282{,}519$; $P < 0.001$) (Fig 2L) of PSDs in the 5th dendritic branching order. Conversely, the PSD area was higher in the remaining branching orders (2nd ($U = 81{,}074$; $P = 0.069$); 3rd ($U = 769{,}008$; $P < 0.001$), and 4th ($U = 1{,}304{,}378$; $P = 0.001$)).

In light of these results, we examined whether the Tau deficiency has additional effects on the morphology of the dendritic spines of 8-week-old newborn neurons, which had shown the most remarkably alterations in PSDs. It should be noted that each dendritic spine can contain one, none, or more than one PSD (Fig EV1A). The absence of Tau increased the density of spines in the 4th branching order dendrites ($U = 232$; $P = 0.022$), whereas a trend to decrease this parameter was observed in 5th branching order dendrites ($t = 1.815$; $P = 0.077$) (Fig EV1B). Moreover, the diameter of the head of the spines located in 5th branching order dendrites was reduced due to Tau deficiency ($U = 177{,}552$; $P < 0.001$) (Fig EV1C). In addition, we classified the dendritic spines into three categories (stubby, thin, and mushroom) and quantified the percentages of each type of spine (Fig EV1D). Tau deficiency reduced the percentage of mushroom spines in 3rd ($\chi^2 = 6.109$; $P = 0.014$) and 5th ($\chi^2 = 12.92$; $P < 0.001$) branching order dendrites. Furthermore, it increased the percentage of stubby spines in the 3rd ($\chi^2 = 7.076$; $P = 0.008$) and that of thin spines in the 5th ($\chi^2 = 8.173$; $P = 0.004$), respectively.

In order to further characterize the morphological alterations caused by Tau deficiency on the postsynaptic elements of granule neurons, we next analyzed the ultrastructure of the afferent synapses in their dendritic spines by electron microscopy (Fig EV2A). This analysis was performed in three separate regions of the molecular layer (ML) of the DG: external (EML), medial (MML), and inner (IML). We found that Tau deficiency reduced the density of synapses (number of synapses per mm^2) in the whole ML ((EML: $t = 2.363$; $P = 0.0019$); (MML: $t = 9.282$; $P < 0.001$); (IML: $t = 2.371$; $P = 0.019$)) (Fig EV2B). Moreover, it increased the size of the synaptic cleft ((EML: $t = -11.216$; $P < 0.001$); (MML: $t = -12.385$; $P < 0.001$); (IML: $t = -8.343$; $P < 0.001$)) (Fig EV2C) and caused alterations in PSDs, which showed a reduced area ((EML: $t = 2.64$; $P = 0.0087$); (MML: $t = 2.322$; $P = 0.021$); (IML: $t = 2.641$; $P = 0.0087$)) (Fig EV2D) and length ((EML: $t = 2.668$; $P = 0.0079$); (MML: $t = 0.818$; $P = 0.413$); (IML: $t = 4.036$; $P < 0.001$)) (Fig EV2E), and an increased depth ((EML: $t = -2.669$; $P = 0.0079$); (MML: $t = -0.488$; $P = 0.625$); (IML: $t = -3.051$; $P = 0.0024$)) (Fig EV2F) than WT ones.

In order to evaluate whether Tau deficiency also has an impact on the morphology of newborn neuron MFTs (efferent synapses), we quantified the area of each individual MFT in 8-week-old retrovirally labeled newborn granule neurons. Figure EV3A and B shows representative images of the whole hippocampus (A), as well as high-power magnifications of MFTs in the CA3 field (B) of WT and Tau$^{-/-}$ mice. No differences were found between WT and Tau$^{-/-}$ animals ($U = 17{,}886$; $P = 0.166$) (Fig EV3C). In addition, and given the high variability in size of the MFT population, we plotted the percentages of MFT grouped by size in WT and Tau$^{-/-}$ mice (Fig EV3D). As shown, no differences in the distribution of MFT sizes were observed to be caused by the absence of Tau (K–S $Z = 1.089$; $P = 0.187$).

Finally, we analyzed the effects of Tau deficiency on the ultrastructure of the MFTs under an electron microscope (Fig EV3E). In this regard, we studied the *stratum lucidum* and *stratum pyramidale* of the CA3 region. The density of presynaptic vesicles (number of vesicles per μm^2) ($t = 3.548$; $P < 0.001$) (Fig EV3F) and the length of the presynaptic active zone ($t = 5.589$; $P < 0.001$) (Fig EV3G) were reduced, whereas the size of the synaptic cleft ($t = -7.409$; $P < 0.001$) (Fig EV3H) was increased in Tau$^{-/-}$ animals compared to WT ones.

In summary, these results suggest that Tau participates in the functional maturation of granule neurons, since its absence alters PSD, dendritic spine, and MFT morphology.

The absence of Tau modifies the electrophysiological properties of granule neurons

In order to determine whether the morphological alterations caused by Tau deficiency affect the basal electrophysiological properties of granule neurons, we recorded the membrane properties and synaptic activity of these cells under whole-cell configuration. Figure 3A and B shows representative traces of miniature excitatory postsynaptic currents (mEPSCs) recorded at a holding potential of −65 mV from WT (black traces) and Tau$^{-/-}$ (red traces) mice. The resting membrane potential of Tau$^{-/-}$ cells was hyperpolarized compared to that of WT cells ($t = 2.217$; $P = 0.038$) (Fig 3C).

We focused our analyses on the mEPSCs to assess whether synaptic inputs were altered by the absence of Tau. Granule cells of the DG of Tau$^{-/-}$ mice did not exhibit alterations in the amplitude ($t = -0.256$; $P = 0.800$) (Fig 3D) neither in the frequency ($U = 53{,}000$; $P = 0.483$) (Fig 3E) of mEPSCs compared to WT ones. However, examination of the cumulative probability distribution of amplitudes of mEPSCs revealed two distinct populations of mEPSCs altered in opposite directions in Tau$^{-/-}$ mice (Fig 3F). Thus, the amplitudes of small mEPSCs of Tau$^{-/-}$ mice were statistically larger than those of WT animals (K–S $Z = 6.306$; $P < 0.001$) (Fig 3F (i)). In contrast, when comparing the mEPSCs of larger amplitudes, those of Tau$^{-/-}$ mice were smaller than those of WT animals (K–S $Z = 9.820$; $P < 0.001$) (Fig 3F (ii)). This result is indicative of a redistribution of excitatory synaptic weights in Tau$^{-/-}$ mice.

Tau protein is required for stress-induced death of newborn granule neurons

Given that AHN is regulated by external stimuli, we next examined whether Tau protein is involved in the negative regulation of AHN exerted by acute stress. We administered CldU thymidine analog to WT and Tau$^{-/-}$ animals in order to label dividing newborn neurons, and then split these animals into two experimental conditions: mice subjected to the Porsolt test (P), which is considered an acute stress model; and control mice not subjected to this test

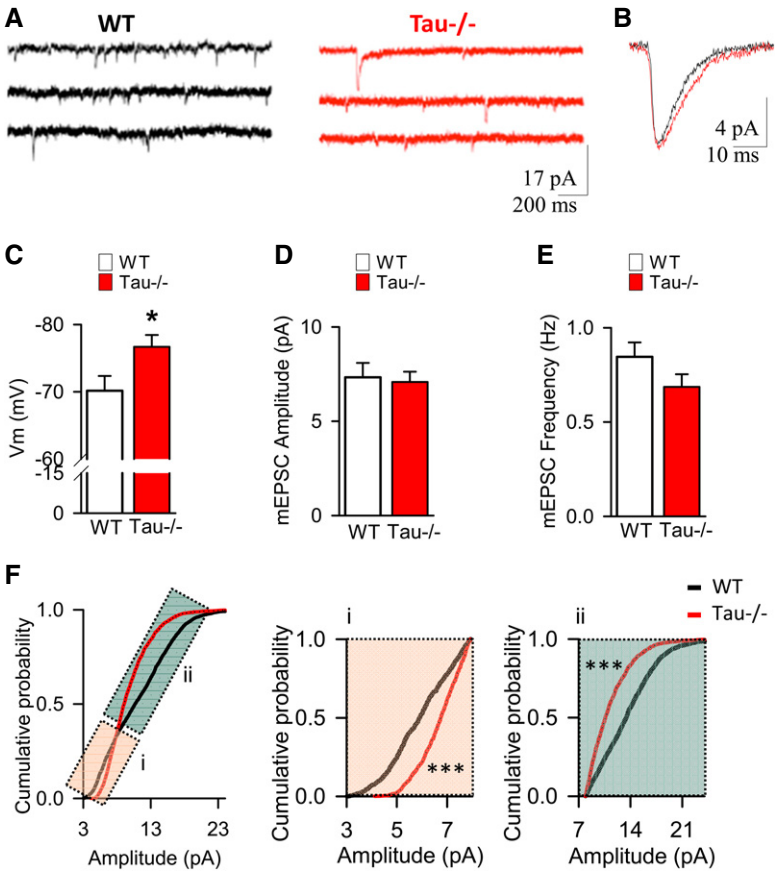

Figure 3. Tau protein deficiency affects basal synaptic activity in granule neurons.

A Representative traces of mEPSCs recorded at a holding potential of −65 mV from WT (black traces) and Tau$^{-/-}$ (red traces) mice.

B Exemplary traces of mEPSCs from one cell from WT (black trace) and Tau$^{-/-}$ (red trace) mice.

C Resting membrane potential of WT and Tau$^{-/-}$ mice (mean ± SEM; $n = 13$ WT cells, $n = 10$ Tau$^{-/-}$ cells; $^*P < 0.05$, Student's t-test).

D, E mEPSC amplitude (D) and mEPSC frequency (E) of WT and Tau$^{-/-}$ animals (mean ± SEM; $n = 13$ WT cells, $n = 10$ Tau$^{-/-}$ cells; Student's t-test or Mann–Whitney U-test).

F Cumulative probability plot of the mEPSC amplitudes, as well as a detailed representation of small (i) and big (ii) mEPSCs from both WT and Tau$^{-/-}$ mice (black and red traces, respectively) ($^{***}P < 0.001$; Kolmogorov–Smirnov Z-test).

(CNP). Animals were sacrificed 1 week after CldU administration. Mice were subjected to the Porsolt test on the 2 days prior to sacrifice (Fig 4A and B). Figure 4C shows representative images of 1-week-old CldU-labeled hippocampal newborn neurons of WT CNP, WT P, Tau$^{-/-}$ CNP, and Tau$^{-/-}$ P mice. The Porsolt test decreased 1-week-old cell survival in both genotypes ($F_{1,52} = 39.14$; $P < 0.001$), but this decrease was higher in WT than in Tau$^{-/-}$ mice (interaction $F_{1,52} = 11.007$; $P = 0.002$) (Fig 4D). These data suggest that the absence of Tau partially protects immature newborn neurons from acute stress-induced cell death. It is important to note that, as previously described (Llorens-Martin & Trejo, 2011), the Porsolt test did not increase the number of

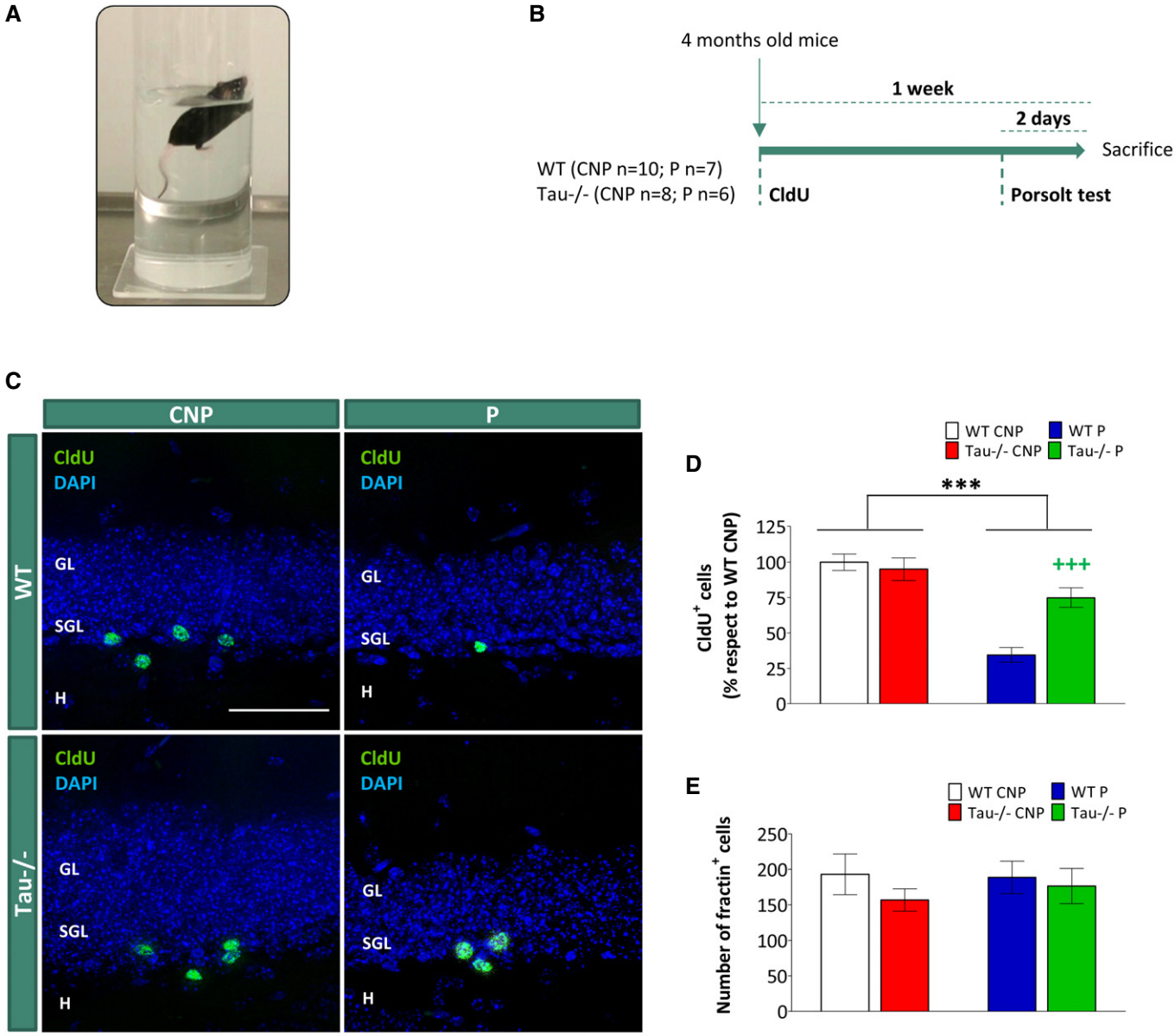

Figure 4. Tau protein is necessary for the stress-induced death of newborn granule neurons.

A Representative image of a mouse subjected to forced swimming in the Porsolt test.

B Schematic diagram of the experimental design.

C Representative images of 1-week-old newborn granule neurons labeled with CldU (green) belonging to WT CNP, WT P, Tau$^{-/-}$ CNP, and Tau$^{-/-}$ P mice. Cell nuclei were labeled with DAPI (blue). Scale bar, 50 μm.

D, E Quantification of the number of 1-week-old CldU^{+} cells (D) and apoptotic fractin^{+} cells (E) in each experimental group.

Data information: The number of animals used is indicated in (B). Data are presented as mean ± SEM. In (D) data are normalized with respect to WT CNP. Black asterisks (*) indicate differences between CNP and P groups: ***$P < 0.001$ (two-way ANOVA). Colored crosses (+) indicate differences between the group represented by the same color and the WT P group: $^{+++}P < 0.001$ (one-way ANOVA + LSD *post hoc* multiple comparisons). GL, granular layer; SGL, subgranular layer; H, hilus. Brightness and contrast of representative confocal microscopy images shown in the figure were minimally adjusted in order to improve visualization.

fractin$^+$ apoptotic cells in either of the genotypes ($F_{1,23} = 0.085$; $P = 0.774$) (Fig 4E).

Tau protein mediates the deleterious effect of stress on newborn granule neuron morphology

With the aim to study the involvement of Tau protein in the morphological alterations triggered by the Porsolt test on newborn granule neurons, we analyzed 8-week-old newborn neurons labeled with PSD95-GFP-expressing retroviruses in WT and Tau$^{-/-}$ mice subjected or not to this test (Fig 5A). Figure 5B shows representative images of neurons in each experimental condition. The Porsolt test reduced the total dendritic length of WT ($P < 0.001$) but not of Tau$^{-/-}$ neurons ($P = 0.623$) (interaction $F_{1,131} = 4.701$; $P = 0.032$) (Fig 5C). Indeed, Tau depletion also partially prevented the alterations in the dendritic branching promoted by the Porsolt test, as revealed by Sholl's analysis. Although acute stress reduced branching between 50 and 100 μm from the soma in both genotypes ($F_{1,133} = 26.19$; $P < 0.001$), it did not cause alterations in any other point of the dendritic tree of Tau$^{-/-}$ neurons (Fig 5D). In contrast, while WT neurons also showed reduced dendritic branching between 100 and 150 μm from the soma ($P = 0.002$), they showed increased dendritic branching between 200 and 250 μm ($P = 0.017$) and between 250 and 300 μm ($P = 0.008$) from the soma.

Tau protein mediates the deleterious effect of stress on the PSDs and MFTs of newborn granule neurons

Figure 5E and F shows representative images of PSDs located in the proximal dendrites of WT CNP, WT P, Tau$^{-/-}$ CNP, and Tau$^{-/-}$ P newborn neurons labeled with PSD95-GFP-expressing retroviruses. In addition to causing alterations in the dendritic morphology of newborn neurons, acute stress also promoted a general decrease in PSD density throughout their whole dendritic tree in WT animals (2nd ($P = 0.019$), 3rd ($P = 0.003$), 4th ($P = 0.005$), and 5th ($P = 0.003$) branching orders). However, in Tau$^{-/-}$ animals, this decrease occurred only in 4th branching order dendrites ($P = 0.007$) (Fig 5G). The average PSD area was not affected by the Porsolt test in WT or in Tau$^{-/-}$ neurons (Fig 5H).

Interestingly, the levels of AMPA receptor GluR1 subunit were decreased in the hippocampus of WT animals after the Porsolt test ($P = 0.006$). However, this decrease was not observed in Tau$^{-/-}$ animals ($P = 0.213$) (Fig 5I and J).

Figure 5K and L shows representative images of the whole hippocampus, together with high-power magnifications of mossy fiber terminals (MFTs) in the CA3 field of WT CNP, WT P, Tau$^{-/-}$ CNP, and Tau$^{-/-}$ P animals. Analysis of the average area of MFTs showed that the effect of acute stress differed in WT and Tau$^{-/-}$ neurons (interaction $F_{1,693} = 7{,}06$; $P = 0.008$). While the Porsolt test reduced the area of MFTs in WT neurons ($P = 0.038$), this effect was not observed in Tau$^{-/-}$ ones (Fig 5M).

Tau protein mediates the pro-neurogenic effects of environmental enrichment (EE)

To test whether Tau protein is also involved in the positive regulation of AHN exerted by EE, we analyzed the survival of 8-week-old adult-generated neurons in WT and Tau$^{-/-}$ animals in control housing (CH) or EE conditions (Fig 6A and B). EE increased the number of DCX$^+$ neuroblasts in both genotypes ($F_{1,33} = 73.12$; $P < 0.001$) (Fig 6C and D). However, analysis of the survival of 8-week-old newborn neuron revealed that the effect was greater in WT than in Tau$^{-/-}$ animals (interaction $F_{1,30} = 7.15$; $P = 0.013$) (Fig 6E and F). Consistent with these data, EE induced a decrease in the number of fractin$^+$ apoptotic cells in both genotypes ($F_{1,32} = 98.10$; $P < 0.001$), but this effect was less pronounced in Tau$^{-/-}$ animals (Fig 6G).

It is known that GABA promotes cell survival during AHN (Song *et al*, 2013). In order to study whether GABAergic innervation is related to the pro-neurogenic effect of EE, we analyzed GAD-65$^+$ GABAergic terminals in the ML of mice in each experimental condition (Fig 7A). The results showed that EE promoted different effects in WT and Tau$^{-/-}$ animals in both the density (interaction

Figure 5. Tau protein mediates the deleterious effect of stress on the dendritic morphology and PSDs of newborn granule neuron.

A Schematic diagram of the experimental design.

B Representative images of 8-week-old newborn granule neurons of WT CNP, WT P, Tau$^{-/-}$ CNP, and Tau$^{-/-}$ P mice infected with a PSD95-GFP-expressing retrovirus. In the WT CNP image, a schematic representation of Sholl's analysis is shown.

C, D Quantification of total dendritic length (C) and Sholl's analysis (D) of 8-week-old newborn granule neurons (n = 3 mice per experimental condition).

E, F Representative images of an 8-week-old newborn granule neuron, in which proximal dendrites are highlighted (E), and of PSDs (green) in proximal dendrites belonging to WT CNP, WT P, Tau$^{-/-}$ CNP, and Tau$^{-/-}$ P mice (F).

G, H Quantification of the number of PSDs/μm (G) and PSD area (H) in each dendritic branching order of 8-week-old newborn granule neurons (n = 3 mice per experimental condition).

I, J Representative Western blot (I) and quantification (J) of the levels of GluR1 subunit of AMPA receptors in hippocampi of WT and Tau$^{-/-}$ mice subjected or not to the Porsolt test (n = 6 mice per experimental condition).

K Representative image showing 8-week-old newborn granule neurons in the DG projecting axons through the mossy fiber tract into the CA3 field (indicated by a white square).

L, M Representative images (L) and quantification of the area (M) of MFTs of 8-week-old newborn neurons in the CA3 region of WT CNP, WT P, Tau$^{-/-}$ CNP, and Tau$^{-/-}$ P mice (n = 3 mice per experimental condition). Arrows indicate MFTs.

Data information: Data are presented as mean ± SEM. In (J) data are normalized with respect to WT CNP. Black asterisks (*) indicate differences between CNP and P groups: ***$P < 0.001$ (two-way ANOVA). Colored asterisks (*) indicate differences between the group represented by the same color and the WT CNP group: *$P < 0.05$, **$P < 0.01$, ***$P < 0.001$; colored crosses (+) indicate differences between the group represented by the same color and the WT P group: $^{+}P < 0.05$, $^{+++}P < 0.001$; colored pads (#) indicate differences between the group represented by the same color and the Tau$^{-/-}$ CNP group: $^{\#\#}P < 0.01$ (one-way ANOVA + LSD *post hoc* multiple comparisons). In representative images, cell nuclei were labeled with DAPI (blue). White scale bars, 50 μm. Red scale bar, 5 μm. Orange scale bar, 300 μm. Green scale bar, 20 μm. Brightness and contrast of representative confocal microscopy images shown in the figure were minimally adjusted in order to improve visualization.

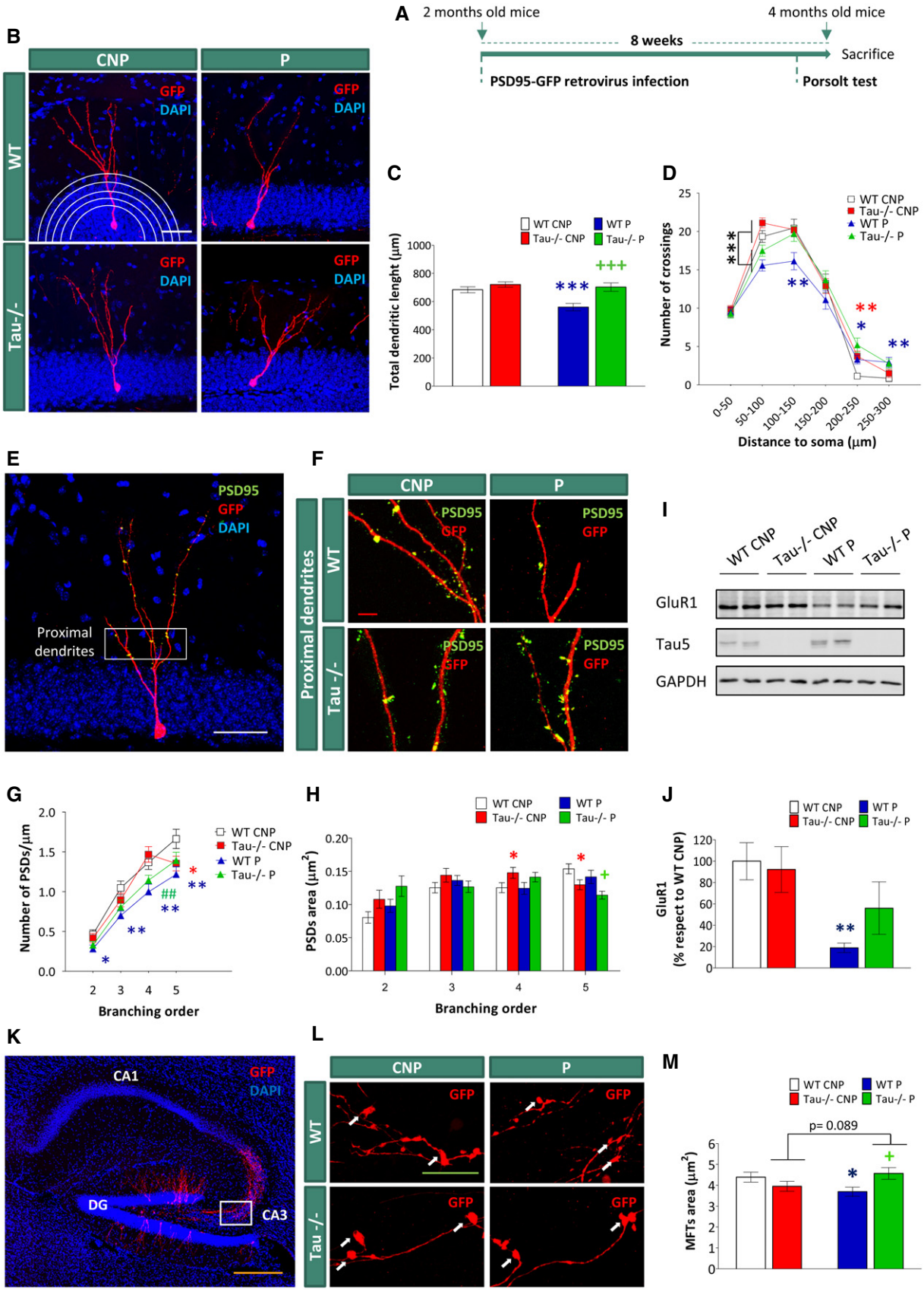
A
2 months old mice
4 months old mice
8 weeks
Sacrifice
PSD95-GFP retrovirus infection
Porsolt test
B
CNP
P
WT
Tau-/-
GFP
DAPI
C
WT CNP
Tau-/- CNP
WT P
Tau-/- P
Total dendritic lenght (µm)
D
Number of crossings
Distance to soma (µm)
0-50
50-100
100-150
150-200
200-250
250-300
E
PSD95
GFP
DAPI
Proximal dendrites
F
Proximal dendrites
I
GluR1
Tau5
GAPDH
G
Number of PSDs/µm
Branching order
H
PSDs area (µm²)
Branching order
J
GluR1 (% respect to WT CNP)
K
CA1
DG
CA3
L
M
MFTs area (µm²)
p= 0.089

Figure 5.

$F_{1,308} = 12.064$; $P = 0.021$) (Fig 7B) and the average area (interaction $F_{1,58527} = 62.406$; $P < 0.001$) (Fig 7C) of GABAergic terminals. While EE promoted an increase in both parameters in WT mice ($P = 0.009$ and $P < 0.001$, respectively), it caused a reduction in both in Tau$^{-/-}$ animals ($P = 0.023$ and $P < 0.001$, respectively). Figure EV4A–D shows the regional changes observed in these parameters in the three subregions of the ML: EML (B), MML (C), and IML (D).

Tau protein mediates the stimulatory effects of EE on newborn neuron morphology

To study whether Tau protein participates in the adaptation of newborn granule neurons to EE, we injected PSD95-GFP-expressing retroviruses into the hippocampus of WT and Tau$^{-/-}$ animals before they were housed under CH or EE conditions for 8 weeks (Fig 8A). EE increased total dendritic length in WT mice ($P = 0.001$), whereas it had no effect on Tau$^{-/-}$ animals ($P = 0.629$) (interaction $F_{1,131} = 4.26$; $P = 0.041$) (Fig 8B and C). Indeed, EE caused an increase in the dendritic branching of WT neurons—an effect not observed in Tau$^{-/-}$ neurons—as revealed by Sholl's analysis (Fig 8D). In particular, this increment occurred between 50 and 100 μm ($P = 0.004$) and between 100 and 150 μm ($P = 0.011$) from the cell soma in WT mice. Thus, EE increased the dendritic length and branching in newborn neurons of WT but not of Tau$^{-/-}$ animals.

Tau protein mediates the stimulatory effects of EE on the PSDs and MFTs of newborn neurons

Figure 8E and F shows representative images of WT and Tau$^{-/-}$ PSDs in distal and proximal dendrites of 8-week-old newborn granule neurons labeled with PSD95-GFP-expressing retroviruses in CH or EE conditions. EE increased PSD density in proximal dendrites of WT neurons compared to WT CH neurons (2^{nd} branching order dendrites $P < 0.001$) (Fig 8G). However, this effect was not observed in Tau$^{-/-}$ neurons (2^{nd} branching order dendrites $P = 0.235$) (interaction $F_{1,132} = 6.839$; $P = 0.010$). Moreover, EE further decreased the density of PSDs in distal dendrites of Tau$^{-/-}$ mice compared to Tau$^{-/-}$ CH mice (5^{th} branching order dendrites $P = 0.006$). In addition, EE decreased the average area of the PSDs in distal dendrites of both genotypes (4^{th} ($F_{1,7109} = 25.98$; $P < 0.001$) and 5^{th} ($F_{1,6960} = 25.27$; $P < 0.001$) branching orders). However, in enriched Tau$^{-/-}$ animals, this decrease also took place in proximal dendrites (2^{nd} ($P < 0.001$) and 3^{rd} ($P < 0.001$) branching orders) (Fig 8H).

Figure 8I and J shows representative images of MFTs in the CA3 region of WT CH, WT EE, Tau$^{-/-}$ CH, and Tau$^{-/-}$ EE animals. EE increased the average area of MFTs in WT ($P = 0.002$) but not in Tau$^{-/-}$ newborn neurons ($P = 0.440$) (Fig 8K).

In summary, EE increased PSD density in proximal dendrites and decreased PSD area in distal dendrites of WT newborn neurons, whereas it decreased PSD density in distal dendrites and reduced PSD area throughout the dendritic tree in Tau$^{-/-}$ newborn neurons. Moreover, EE caused an increment in the area of MFTs of WT newborn neurons. This observation was not made in the absence of Tau.

Finally, a schematic model illustrating the effects of the absence of Tau on the modulation of AHN by external stimuli is shown in Fig 9.

Discussion

Tau is involved in the morphological and functional maturation of newborn granule neurons under basal conditions

Tau protein is crucial for the establishment of neuronal polarity during embryonic development, for axonal transport, and for the intracellular trafficking of various molecules (Caceres & Kosik, 1990; Dawson *et al*, 2001; de Barreda *et al*, 2010; Hernandez & Avila, 2010; Llorens-Martin *et al*, 2011; Sapir *et al*, 2012). Given the tight control of Tau expression during AHN, it is reasonable to assume that this protein plays a regulatory role in this process. However, despite the widespread expression of Tau during AHN (Fuster-Matanzo *et al*, 2009), none of the cellular subpopulations studied was affected by the absence of Tau. Strikingly, here we demonstrate that Tau depletion causes a transient alteration in the morphology of adult newborn neurons. Our data are consistent with those of previous reports showing a delayed morphological maturation of embryonic neurons both *in vitro* (Dawson *et al*, 2001) and *in vivo* (Sapir *et al*, 2012). Our results show that Tau knockout reduced the total dendritic length and branching of 4-week-old newborn granule neurons, a phenomenon not observed in 8-week-old newborn neurons. These data suggest that other microtubule-associated proteins play compensatory roles at later stages of newborn neuron maturation. In line with the former notion, a compensatory role of MAP1A has been described in these mice (Harada *et al*, 1994).

In addition to the dendritic alterations, the absence of Tau affected newborn granule neuron PSDs. Tau knockout specifically

Figure 6. Tau protein mediates the pro-neurogenic effects of environmental enrichment.

A Representative images of control housing (CH) and environmental enrichment (EE) cages.

B Schematic diagram of the experimental design.

C, D Representative images of DCX$^+$ cells in the DG of CH and EE animals (C) and quantification of the number of DCX$^+$ cells of WT and Tau$^{-/-}$ animals in CH or EE conditions (D).

E Representative images of 8-week-old newborn granule neurons labeled with IdU (red) belonging to WT CH, WT EE, Tau$^{-/-}$ CH, and Tau$^{-/-}$ EE mice.

F, G Quantification of the number of 8-week-old IdU$^+$ cells (F) and apoptotic fractin$^+$ cells (G).

Data information: The number of animals used is indicated in (B). Data are presented as mean ± SEM. In (F), data are normalized with respect to WT CH. Black asterisks (*) indicate differences between CH and EE groups: ***$P < 0.001$ (two-way ANOVA). Colored asterisks indicate differences between the group represented by the same color and the WT CH group: **$P < 0.01$, ***$P < 0.001$; colored crosses (+) indicate differences between the group represented by the same color and the WT EE group: $^+P < 0.05$, $^{++}P < 0.01$ (one-way ANOVA + LSD *post hoc* multiple comparisons). GL, granular layer; SGL, subgranular layer; H, hilus; ML, molecular layer. In representative images, cell nuclei were labeled with DAPI (blue). White scale bar, 20 μm. Red scale bar, 50 μm. Brightness and contrast of representative confocal microscopy images shown in the figure were minimally adjusted in order to improve visualization.

reduced not only the number but also the area of most distal PSDs (located on 5th branching order dendrites) in these neurons. In addition, it decreased the percentage of mushroom spines and the spine head diameter in the aforementioned dendrites. These data might be relevant given that the main afferent pathway in the DG is composed by the axons of the pyramidal neurons of the entorhinal cortex (EC) (the perforant pathway). This pathway preferentially ends in the two outer thirds of the ML, where the 5th branching order dendrites of the granule neurons are located. Moreover, Tau deficiency also triggered ultrastructural alterations in the afferent

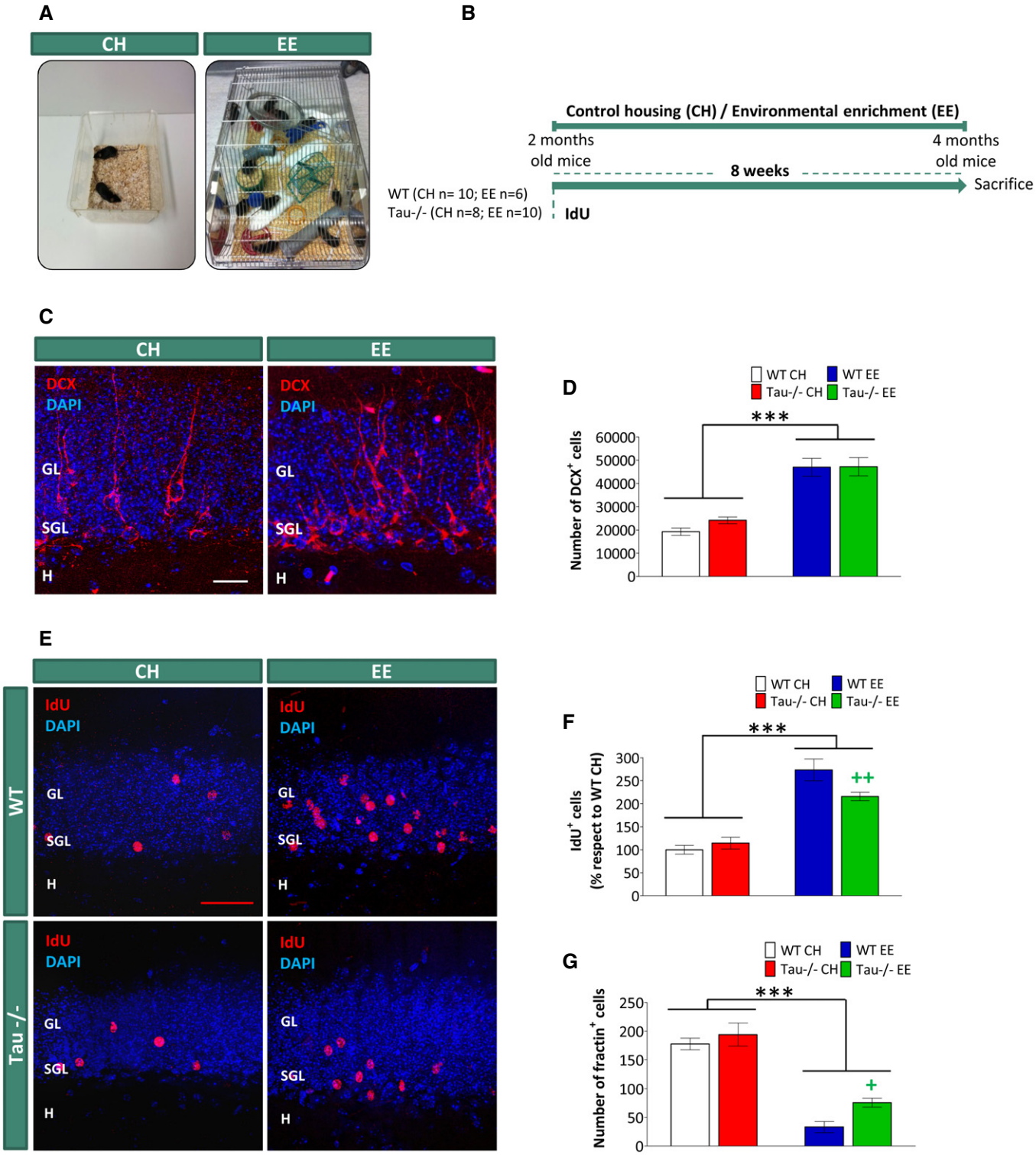

Figure 6.

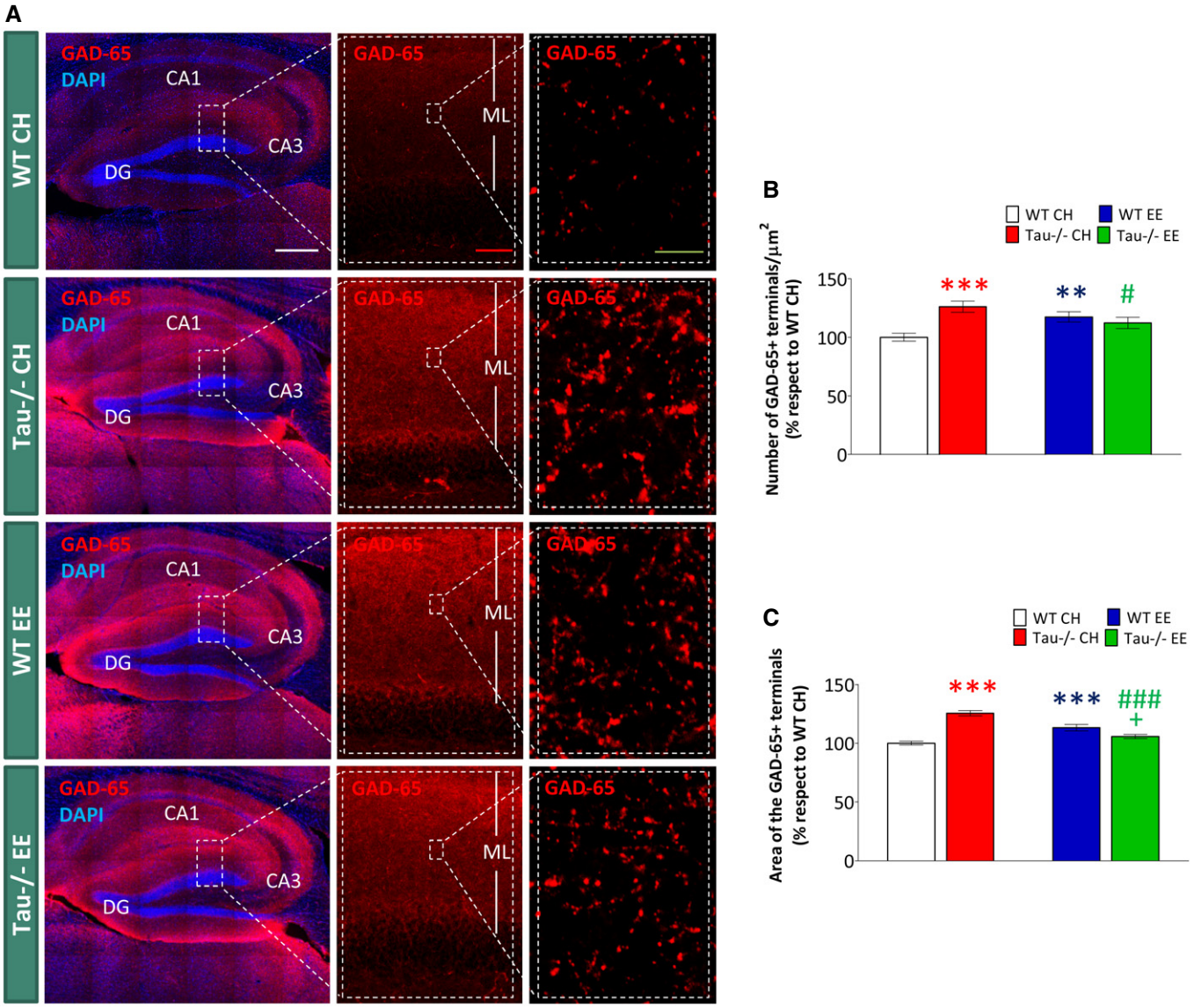

Figure 7. Tau protein is involved in the effect of EE on GABAergic innervation.

A Representative images of the whole hippocampus showing GABAergic innervation labeled with GAD-65 antibody (red), and high-power magnifications of the DG molecular layer showing GAD-65$^+$ terminals in WT CH, Tau$^{-/-}$ CH, WT EE, and Tau$^{-/-}$ EE mice. Cell nuclei were labeled with DAPI (blue). White scale bar, 300 µm. Red scale bar, 50 µm. Green scale bar, 5 µm.

B, C Quantification of the density (B) and area (C) of GAD-65$^+$ terminals in the molecular layer of mice in each experimental condition (n = 10 WT CH mice, n = 8 Tau$^{-/-}$ CH mice, n = 6 WT EE mice, n = 10 Tau$^{-/-}$ EE mice).

Data information: In (B, C) data are presented as mean ± SEM (normalized with respect to WT CH). Colored asterisks indicate differences between the group represented by the same color and the WT CH group: $^{**}P < 0.01$, $^{***}P < 0.001$; colored crosses (+) indicate differences between the group represented by the same color and the WT EE group: $^{+}P < 0.05$; colored pads (#) indicate differences between the group represented by the same color and the Tau$^{-/-}$ CH group: $^{\#}P < 0.05$, $^{\#\#\#}P < 0.001$ (one-way ANOVA + LSD *post hoc* multiple comparisons). DG, dentate gyrus; ML, molecular layer.

synapses of granule neurons. An enlargement in both the synaptic cleft and the depth of the PSDs was detected. This observation may indicate the destabilization of these elements caused by Tau deficiency. In addition, we showed that absence of this protein also alters the ultrastructure of MFTs (efferent synapses), which may have important consequences for granule neuron functionality.

Indeed, electrophysiological recordings showed that the granule neurons of Tau$^{-/-}$ mice exhibit a hyperpolarized resting membrane potential. Moreover, with respect to synaptic strength, we observed a bidirectional effect in Tau-deficient neurons, in which smaller mEPSCs got larger, and conversely, the larger mEPSCs got smaller. The molecular basis for these alterations is unclear, but they are indicative of a redistribution of synaptic weights, which is consistent with the bidirectional effect of PSD size that we also observed in these neurons. In fact, Tau is present in dendritic spines (Ittner *et al*, 2010; Mondragon-Rodriguez *et al*, 2012; Frandemiche *et al*, 2014).

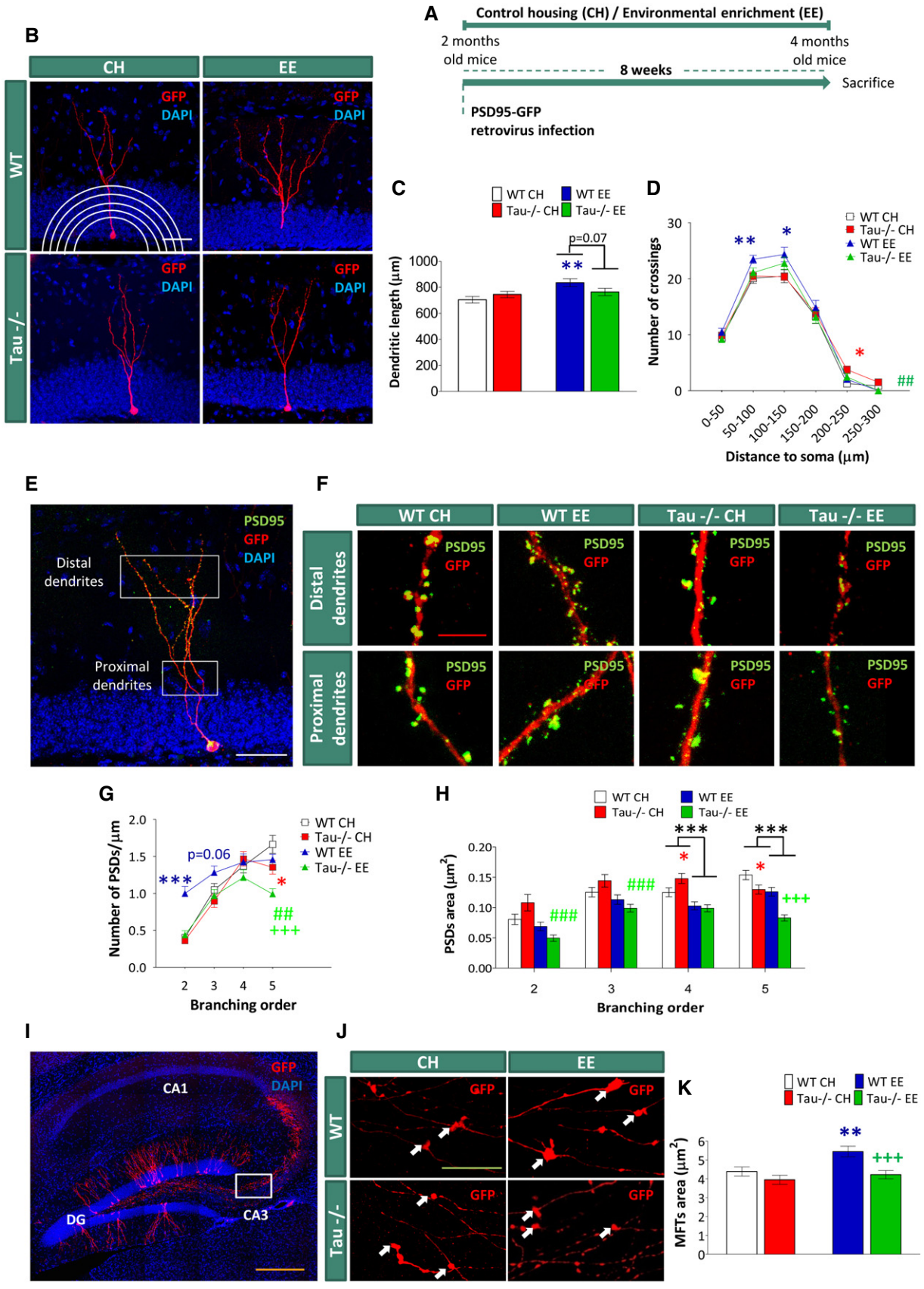
A
Control housing (CH) / Environmental enrichment (EE)
2 months old mice
4 months old mice
8 weeks
Sacrifice
PSD95-GFP retrovirus infection
B
CH
EE
WT
Tau -/-
GFP
DAPI
C
WT CH
WT EE
Tau-/- CH
Tau-/- EE
p=0.07
Dendritic length (µm)
D
Number of crossings
Distance to soma (µm)
0-50
50-100
100-150
150-200
200-250
250-300
E
PSD95
GFP
DAPI
Distal dendrites
Proximal dendrites
F
WT CH
WT EE
Tau -/- CH
Tau -/- EE
Distal dendrites
Proximal dendrites
G
Number of PSDs/µm
p=0.06
Branching order
H
PSDs area (µm²)
Branching order
I
CA1
DG
CA3
J
K
MFTs area (µm²)

Figure 8.

Figure 8. Tau protein mediates the stimulatory effects of EE on the dendritic morphology, PSDs, and MFTs of newborn neurons.

A Schematic diagram of the experimental design.

B Representative images of 8-week-old newborn granule neurons of WT CH, WT EE, $Tau^{-/-}$ CH, and $Tau^{-/-}$ EE mice infected with a PSD95-GFP-expressing retrovirus. In the WT CH image, a schematic representation of Sholl's analysis is shown.

C, D Quantification of total dendritic length (C) and Sholl's analysis (D) of 8-week-old newborn granule neurons (n = 3 mice per experimental condition).

E, F Representative images of an 8-week-old newborn granule neuron in which proximal and distal dendrites are highlighted (E) and of PSDs (green) in distal and proximal dendrites of WT and $Tau^{-/-}$ mice housed under either CH or EE conditions (F).

G, H Quantification of the number of PSDs/μm (G) and PSD area (H) in each dendritic branching order of 8-week-old newborn granule neurons (n = 3 mice per experimental condition).

I Representative image showing 8-week-old newborn granule neurons in the DG projecting axons through the mossy fiber tract into the CA3 field (indicated by a white square).

J, K Representative images (J) and quantification of the area (K) of MFTs of 8-week-old newborn neurons in the CA3 region of WT CH, WT EE, $Tau^{-/-}$ CH, and $Tau^{-/-}$ EE mice (n = 3 mice per experimental condition). Arrows indicate MFTs.

Data information: Data are presented as mean ± SEM. Black asterisks (*) indicate differences between CH and EE groups: ***$P < 0.001$ (two-way ANOVA). Colored asterisks indicate differences between the group represented by the same color and the WT CH group: *$P < 0.05$, **$P < 0.01$, ***$P < 0.001$; colored crosses (+) indicate differences between the group represented by the same color and the WT EE group: $^{+++}P < 0.001$; colored pads (#) indicate differences between the group represented by the same color and the $Tau^{-/-}$ CH group: $^{\#\#}P < 0.01$, $^{\#\#\#}P < 0.001$ (one-way ANOVA + LSD *post hoc* multiple comparisons). In representative images, cell nuclei were labeled with DAPI (blue). White scale bars, 50 μm. Red scale bar, 5 μm. Orange scale bar, 300 μm. Green scale bar, 20 μm. Brightness and contrast of representative confocal microscopy images shown in the figure were minimally adjusted in order to improve visualization.

In these structures, it has been shown that activation of NMDA glutamate receptor triggers Tau phosphorylation, thus regulating the interaction of Tau with the actin cytoskeleton, PSD95, and Fyn kinase (Ittner *et al*, 2010; Mondragon-Rodriguez *et al*, 2012; Frandemiche *et al*, 2014). Interestingly, the basal subtle electrophysiological alterations described in this work seem to occur specifically in granule neurons, as it has been demonstrated that Tau deficiency does not affect basic synaptic currents in other regions of the brain (Ittner *et al*, 2010). Thus, it can be hypothesized that granule neurons are selectively affected by Tau deficiency in terms of their basal synaptic activity. In addition, alterations that may be related to deficient synaptic plasticity (LTP and LTD) have been reported in $Tau^{-/-}$ mice (Ahmed *et al*, 2014; Kimura *et al*, 2014; Regan *et al*, 2015). In fact, hippocampal LTD is considered necessary for clearing old memories, and $Tau^{-/-}$ mice show impairments in learning flexibility and various types of hippocampal-dependent memory (Ikegami *et al*, 2000; Ahmed *et al*, 2014; Lei *et al*, 2014; Ma *et al*, 2014; Regan *et al*, 2015). Remarkably, it has been described that granule neurons are important for flexibility of learning strategies (Garthe *et al*, 2009).

Tau mediates the deleterious effects of acute stress on newborn neurons

Tau absence confers neuroprotection in several models of neuronal damage, such as traumatic brain injury (Cheng *et al*, 2014), neuroinflammation (Maphis *et al*, 2015), amyloid β-mediated excitotoxicity (Roberson *et al*, 2007, 2011; Ittner *et al*, 2010; Vossel *et al*, 2010), and epilepsy (Holth *et al*, 2013), among others. Given that acute stress negatively affects AHN (Gould *et al*, 1992) and considering the neuroprotection exerted by the lack of Tau in the aforementioned models, we addressed whether the Porsolt test would cause similar detrimental effects in $Tau^{-/-}$ and WT mice.

The Porsolt test causes selective cell death of 1-week-old newborn neurons but does not cause a net increase in general apoptosis in the DG (Llorens-Martin & Trejo, 2011). We found that the reduction of newborn neuron survival was less pronounced in $Tau^{-/-}$ compared to WT mice, thereby suggesting a certain degree of neuroprotection against neuronal death triggered by forced swimming in the former. Of note, this phenomenon is not attributable to an ineffectiveness of the Porsolt test on $Tau^{-/-}$ mice, as immobility time scores were similar in both genotypes. Interestingly, cell death triggered by forced swimming is mediated by glutamate excitotoxicity (Moghaddam *et al*, 1994; Nair & Bonneau, 2006), a phenomenon that $Tau^{-/-}$ neurons are protected against (Ittner *et al*, 2010).

In addition, we also found that while the Porsolt test decreased the total dendritic length and branching of WT neurons, it caused no alterations to the morphology of $Tau^{-/-}$ neurons. Moreover, forced swimming reduced the number of PSDs in WT mice, while it did not cause remarkable variations in $Tau^{-/-}$ animals. Indeed, although forced swimming reduced the average area of the MFTs in WT neurons, it did not cause this effect in $Tau^{-/-}$ ones. These data are in agreement with the relevant role played by Tau at the presynaptic compartment (Decker *et al*, 2015; Sokolow *et al*, 2015). Altogether, our findings support the above-indicated notion that newborn granule neurons are, to some extent, protected from the detrimental consequences of the Porsolt test.

One of the mechanisms triggered by this test is the decrease in the levels of GluR1 subunit of AMPA receptors (Groc *et al*, 2008;

Figure 9. Schematic model.

A Under basal conditions, Tau protein is involved in the maturation of newborn granule neurons in the DG. In the absence of Tau, newborn neuron dendritic arborization is transiently altered and PSD formation is impaired (decreased PSD density and area were found in the distal dendrites).

B Acute stress decreases the survival of immature 1-week-old newborn granule neurons, an effect that is less pronounced in $Tau^{-/-}$ animals as compared to WT. Furthermore, acute stress also impairs dendritic branching and reduces PSD density and MFT area in 8-week-old fully mature newborn neurons of WT animals. In contrast, these effects are not observed in $Tau^{-/-}$ mice.

C EE increases 8-week-old mature newborn neuron survival, dendritic branching, MFT area, and PSD density in the proximal dendrites, whereas it decreases PSD area in the distal dendrites of WT neurons. However, these effects are less pronounced or even inexistent in the absence of Tau. Actually, EE further reduces the density and area of the PSDs in $Tau^{-/-}$ distal dendrites.

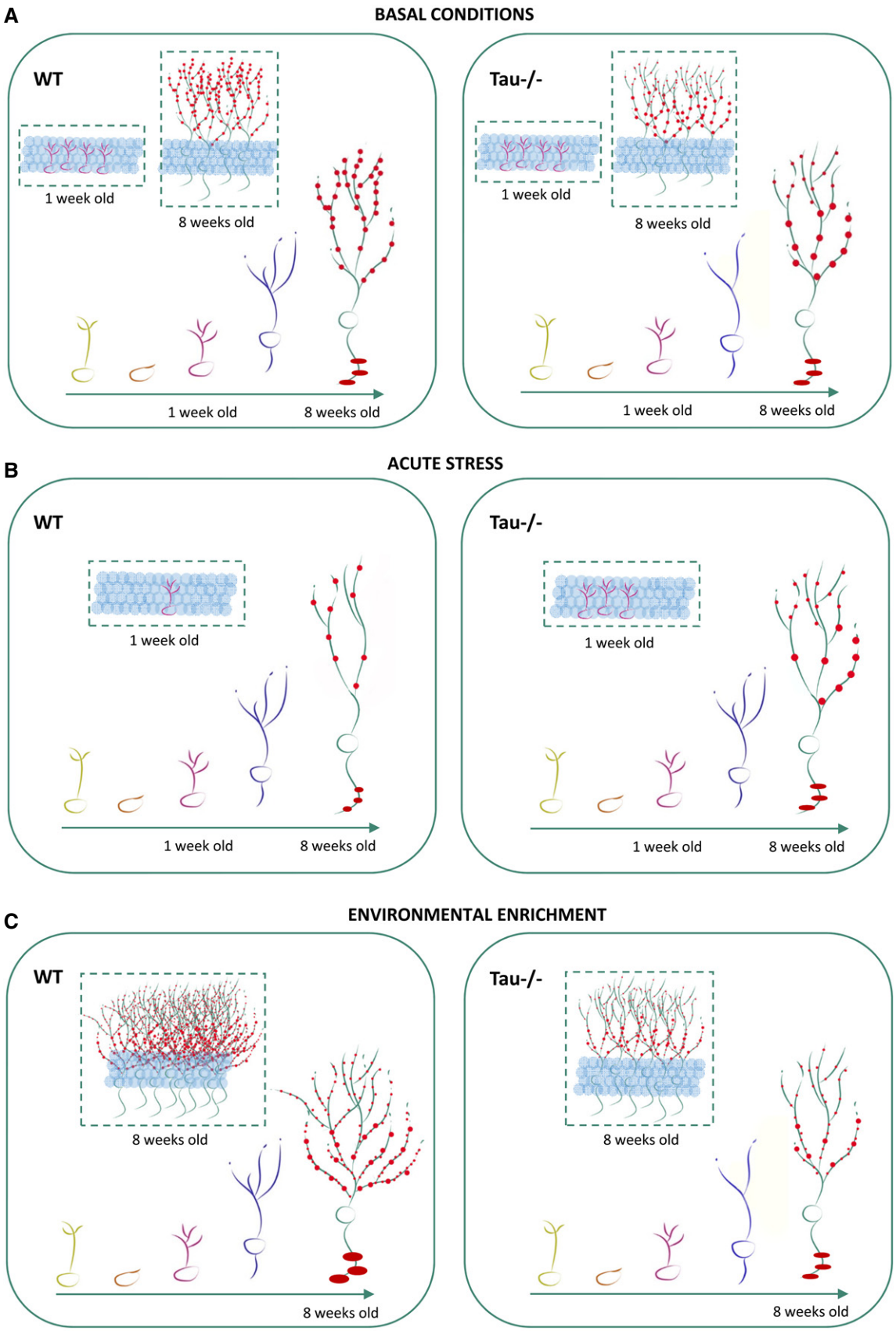

Figure 9.

Llorens-Martin & Trejo, 2011). Given the growing relevance of AMPA receptor-modulating compounds (known as AMPAkines) in the treatment of major depression (Bai *et al*, 2003; Arai & Kessler, 2007), we addressed whether the reduction in AMPA receptor expression caused by acute stress occurs in both genotypes in the same manner. Indeed, this effect was not detected in $Tau^{-/-}$ animals. In this regard, Regan *et al* (2015) demonstrated that $Tau^{-/-}$ mice present basal deficits in AMPA internalization. This observation is in agreement with our results, since we observed unchanged levels of GluR1 in these mice after the Porsolt test. Given that AMPA receptor internalization triggers dendritic spine disappearance (Collingridge *et al*, 2004), it can be hypothesized that the impairment in this mechanism explains the unchanged number of PSDs in $Tau^{-/-}$ mice. Furthermore, it could be related to the neuroprotection shown in newborn neurons against forced swimming.

Tau regulates the effects of EE on adult hippocampal neurogenesis

Environmental enrichment is one of the strongest positive regulators of AHN (Kempermann *et al*, 1997). Given the alterations observed in newborn neurons of $Tau^{-/-}$ mice, we examined whether EE would trigger similar stimulatory effects on AHN in both genotypes. EE triggered a similar increase in the number of DCX^+ neuroblasts in WT and $Tau^{-/-}$ mice, thereby demonstrating that EE causes a general stimulatory effect in the hippocampus. However, the stimulatory effect of EE in 8-week-old newborn neuron survival in $Tau^{-/-}$ mice was less pronounced than in WT animals. In this regard, it has been demonstrated that some of the neuroprotective actions of EE are exerted through an increase in BDNF (Hu *et al*, 2013), and the actions of which are mediated by GABA (Waterhouse *et al*, 2012). Interestingly, we observed increased GABAergic innervation in the ML of the WT hippocampus in response to EE but not in that of $Tau^{-/-}$ animals.

Furthermore, analysis of the morphology of $Tau^{-/-}$ newborn neurons suggested an impaired capacity to detect the increased demand for information processing caused by EE. This stimulus increased total dendritic length and branching in WT newborn neurons, a phenomenon previously described (Llorens-Martin *et al*, 2013). However, no increase in these parameters was observed in enriched $Tau^{-/-}$ mice. Thus, although fully mature newborn granule neurons did not differ morphologically between the two genotypes under CH conditions, we propose that the cytoskeleton of $Tau^{-/-}$ neurons lack, to some extent, the plasticity needed to adapt to the stimulatory actions of EE.

It is noteworthy that one of the most challenging features of EE is that both permanent elements (such as the size and shape of the cage) and similar but changing ones (interchangeable objects and toys) must be constantly remembered and or/newly memorized by the animal. Given that the whole environment is changed periodically during the enrichment period, both the formation and clearance of new memories are probably required. In line with this, the lifetime of hippocampal synapses matches the longevity of hippocampal memories (Attardo *et al*, 2015), and EE increases both LTD and LTP (Artola *et al*, 2006).

Importantly, EE resulted in a net increase in the density and a reduced area of PSDs in WT newborn neurons. It has been suggested that this phenomenon is caused by the resulting addition of newly generated, small, synaptic contacts (Llorens-Martin *et al*, 2013). In contrast, EE reduced the number and size of the PSDs located on the 5^{th} branching order dendrites of $Tau^{-/-}$ neurons, which were already reduced under CH conditions in comparison with those of WT mice. Given that $Tau^{-/-}$ mice present impairments in both LTP (Ahmed *et al*, 2014) and LTD (Kimura *et al*, 2014), the reduction in the number and size of 5^{th} branching order PSDs in response to EE may be the consequence of two events. On one hand, due to inefficient LTP generation, EE might not be able to trigger a net increase in the formation of new PSDs. On the other hand, due to deficient LTD induction, the reduced clearance of old synaptic contacts may harness their replacement by newly generated synaptic contacts, a phenomenon that controls newborn neuron integration into the hippocampal circuit (Toni & Sultan, 2011).

Tau is translocated to the postsynaptic compartment of dendrites in response to synaptic stimulation (Mondragon-Rodriguez *et al*, 2012; Frandemiche *et al*, 2014). Moreover, it has been suggested that the presence and interaction of microtubules at synaptic spines is crucial for the BDNF-triggered addition of new synaptic contacts during development (Gu *et al*, 2008) and that microtubule dynamics control the shape and maturation of synaptic spines (Hu *et al*, 2008; Jaworski *et al*, 2009). Thus, it is reasonable to assume that the putative alterations of microtubule cytoskeleton plasticity, as well as the weakness of PSDs caused by the absence of Tau, may be related to the impaired enhancement of synaptic plasticity triggered by EE in $Tau^{-/-}$ mice. In addition, analysis of newborn neuron MFTs revealed that while EE increased the average area of MFTs in WT mice, it did not cause any change in $Tau^{-/-}$ neurons. These observations would suggest that $Tau^{-/-}$ presynaptic structures also show impaired plasticity.

Concluding remarks

Taken together, our data suggest that Tau plays a novel role in the maturation of newborn granule neurons *in vivo* under basal conditions. Furthermore, we provide evidence that Tau regulates the effects of external stimuli on AHN. In addition to other forms of neuroprotection caused by the absence of Tau, here we show that this protein mediates the deleterious effects of acute stress on AHN. Furthermore, we demonstrate, for the first time, that Tau modulates the stimulatory actions of EE on newborn neurons. All together, these data shed light on novel functions of Tau protein related to the plastic modulation of AHN by external stimuli, which, to the best of our knowledge, have not been demonstrated for any other protein in the AHN model.

Materials and Methods

Animals

$Tau^{-/-}$ mice were generated as previously described (Dawson *et al*, 2001). Heterozygous ($Tau^{+/-}$) mice were crossed in order to obtain homozygous Tau knockout mice ($Tau^{-/-}$) and control littermates (WT). Mice were housed at the Centro de Biología Molecular "Severo Ochoa" animal facility under standard laboratory conditions, in accordance with European Community Guidelines (directive 86/609/EEC), and were handled complying with European and

local animal care protocols. Six to ten animals per experimental condition and time point were used for histological and biochemical determinations. Three animals per experimental condition and time point were used for retroviral labeling, electrophysiological recordings, and electron microscopy analyses. Animals were sacrificed at 4 months of age.

Administration of thymidine analogs

The thymidine analogs CldU and IdU (Sigma-Aldrich, St. Louis, MO) were used to analyze the survival of 1-, 2-, 4-, 6-, and 8-week-old newborn granule neurons. CldU was administered in a single intraperitoneal injection of 42.75 mg/kg. IdU was administered over 24 h diluted in drinking water at 0.92 mg/ml. These doses were based on equimolar doses of 50 mg/kg (Llorens-Martin *et al*, 2010) and 0.8 mg/ml BrdU (Lugert *et al*, 2010), respectively.

Retroviral stock preparation

We used a retroviral stock (PSD95-GFP) encoding for PSD95 fused to GFP (Kelsch *et al*, 2008). The PSD95-GFP retrovirus allowed PSD visualization (green channel). Moreover, anti-GFP immunohistochemistry (red channel) allowed visualization of the whole neuronal morphology (Kelsch *et al*, 2008). The plasmids used to produce the PSD95-GFP retrovirus were kindly provided by Prof. Carlos Lois (University of Massachusetts). Retroviral stocks were concentrated to working titers of 1×10^7–2×10^8 pfu/ml by ultracentrifugation (Zhao *et al*, 2006). Since the retroviruses used are engineered to be replication incompetent, only dividing cells at the time of surgery can be infected (Zhao *et al*, 2006; Kelsch *et al*, 2008).

Stereotaxic surgery

Mice were anesthetized with isoflurane and placed in a stereotaxic frame. Coordinates (mm) relative to bregma in the anteroposterior, mediolateral, and dorsoventral axes were as follows: dentate gyrus (DG) [−2.0, 1.4, 2.2]. Two μl/DG of virus solution was infused at 0.2 μl/min via a glass micropipette. Mice were 8 weeks old at the time of retroviral injections.

Environmental enrichment (EE)

We used a previously described EE protocol (Llorens-Martin *et al*, 2010). Enriched mice were housed in groups of 10 animals for 8 weeks in large transparent polycarbonate cages (55_33_20 cm, Plexx Ref. 13005). All enriched cages were equipped with various types of running wheels. The mice had free access to toys of different shapes, sizes, materials, and surface texture. Every other day, a set of 10–15 different toys and new bedding were placed in the cages in order to change the whole environment, as previously described (Llorens-Martin *et al*, 2010).

Forced swimming (the Porsolt test)

Animals were placed in a 12-cm-diameter and 29-cm-tall cylinder filled with water at 23°C for 6 min on two consecutive days (Detke *et al*, 1995). Acute stress induced by forced swimming led to depressive-like behavior in mice.

Morphometric analysis of newborn granule neurons

Three series of sections from each PSD95-GFP retrovirus-injected animal were used for the immunohistochemical detection of GFP. Thirty randomly selected neurons from each experimental condition were reconstructed under a LSM710 Zeiss confocal microscope (25× oil immersion objective). Confocal stacks of images were obtained (*Z*-axis interval: 2 μm), and Z-projections were analyzed for the determination of total dendritic length and Sholl's analysis. All cells were traced using *NeuronJ* plugin for ImageJ software. Sholl's analysis was performed using the plugin *ShollAnalysis* for ImageJ. This analysis consists on placing a central point on the cell soma and tracing concentric circles (separated by a 10-μm distance interval). The number of times that the dendritic tree intersects each circle is represented in the graphs (number of crossings).

Number and area of PSDs of newborn granule neurons

The number and area of PSD95-GFP$^+$ clusters were analyzed separately for each branching order in the dendritic tree of retrovirus-labeled newborn neurons. A minimum of 30 segments belonging to each experimental condition were analyzed for each branching order. Confocal stacks of images were obtained in a LSM710 Zeiss confocal microscope (63× oil immersion objective; XY dimensions: 67.4 μm; z-axis interval: 0.2 μm). Two-channel stack Z-projections were obtained. The dendritic length of each segment was measured (red channel, GFP), and the number and area of PSD-GFP$^+$ clusters were analyzed using the semi-automatic *Particle Analyzer* plugin for ImageJ (green channel, PSD95).

Area of MFTs of newborn granule neurons

The area of individual MFTs labeled with GFP was measured in the CA3 region of PSD95-GFP retrovirus-injected animals. A minimum of 20 stacks of images per experimental condition were obtained in a LSM710 Zeiss confocal microscope (63× oil immersion objective; XY dimensions: 100 μm; Z-interval: 0.5 μm). Stacks were randomly obtained among the different sections composing the series. GFP-Z-projections were obtained, and the area of each MFT was measured manually in ImageJ software, as previously described (Toni *et al*, 2008). The following criteria were selected for MFT quantification: (i) the diameter of the MFT is more than threefold greater than the diameter of the axon; (ii) the MFT is connected to the axon on at least one end; and (iii) the MFT is relatively isolated from other MFTs for accuracy of tracing (Toni *et al*, 2008). Given that the MFTs of the CA2 region are significantly smaller than those of the CA3 (Llorens-Martin *et al*, 2015), we avoided the CA2 region when obtaining the images. All the measurements were made in equivalent rostrocaudal positions of the CA3 field that were always closer to the hilus than to the CA2 region. A minimum of 100 MFTs per experimental condition were measured.

Statistical analysis

Statistical analysis was performed using the SPSS 22 software (SPSS, 1989; Apache Software Foundation, Chicago, IL, USA). The Kolmogorov–Smirnov test was used to test the normality of the sample distribution. Atypical data were detected with box plots and

eliminated when necessary. For comparisons between 2 experimental groups, date from cell counts (PH3, fractin, Sox2, DCX, thymidine analog survival, BLBP, and calretinin), morphometric analysis (total dendritic length and Sholl's analysis), analysis of the PSDs in newborn neurons under a confocal microscope (density and area of PSDs), analysis of dendritic spines under a confocal microscope (density and head diameter of dendritic spines), electron microscopy analysis (number of presynaptic vesicles, length of the active zone, synaptic cleft size, PSD length, depth, and area), and electrophysiological recordings were analyzed by a Student's *t*-test in the case of normal sample distribution or by a nonparametric test (Mann–Whitney *U*-test) in those cases in which normality could not be assumed. For comparisons between more than 2 experimental groups (Western blot quantifications, thymidine analog experiments, cell counts, GABAergic innervation, morphometric analysis, and analysis of the PSDs when analyzed in either stressed or enriched mice), data were analyzed by a two-way ANOVA test. In those cases in which the two-way ANOVA interaction was statistically significant, a one-way ANOVA followed by a Fischer LSD *post hoc* analysis was used to compare the differences between individual groups. Graphs represent mean values ± SEM. The percentage of the different types of dendritic spines of newborn neurons, as well as the percentage of cells expressing DCX and NeuN, were analyzed by a chi-squared (χ^2) test. The comparison between the cumulative distributions of amplitudes of mEPSCs, as well as the comparison between the distributions of MFT sizes, was performed by a Kolmogorov–Smirnov *Z*-test.

A detailed methodological description of the sacrifice and tissue processing, immunohistochemistry, cell counting, analysis of GABAergic innervation, morphometric analysis of the dendritic spines of newborn granule neurons, electron microscopy, Western blot, and electrophysiological recordings are provided in Appendix Supplementary Methods.

Expanded View for this article is available online.

Acknowledgements
This work was supported in part by grants from the Alzheimer's Association (2015-NIRG-340709) (M. Llorens-Martín), the Ministerio de Economia y Competitividad (SAF-2014-5040-P, J. Ávila; BUF2013-40664-P, F. Hernández; SAF2014-58598-JIN, M. Navarrete; SAF2014-57233-R, Jose A. Esteban), and from the Centro de Investigación Biomédica en Red sobre Enfermedades Neurodegenerativas (CIBERNED, ISCIII) (J. Ávila). The authors thank E. García for help producing retroviral vectors, C. Lois for providing the plasmids used for the production of the PSD95-GFP virus, and R. Cuadros for the technical assistance with WBs and electron microscopy. The authors also thank the "Servicio de Microscopía Óptica y Confocal" of the CBMSO for their help with confocal microscopy.

Author contributions
NPB performed and supervised all the experiments. MLLM performed the electron microscopy experiments. JJA performed the retroviral injections. MN performed and analyzed the electrophysiological experiments. JAE supervised the electrophysiological experiments. MLLM, JA, FH, MN, and JAE obtained funding. NPB, MLLM, and JA wrote the manuscript.

Conflict of interest
The authors declare that they have no conflict of interest.

References

Ahmed T, Van der Jeugd A, Blum D, Galas MC, D'Hooge R, Buee L, Balschun D (2014) Cognition and hippocampal synaptic plasticity in mice with a homozygous tau deletion. *Neurobiol Aging* 35: 2474 – 2478

Aimone JB, Deng W, Gage FH (2011) Resolving new memories: a critical look at the dentate gyrus, adult neurogenesis, and pattern separation. *Neuron* 70: 589 – 596

Andreadis A, Brown WM, Kosik KS (1992) Structure and novel exons of the human tau gene. *Biochemistry* 31: 10626 – 10633

Arai AC, Kessler M (2007) Pharmacology of ampakine modulators: from AMPA receptors to synapses and behavior. *Curr Drug Targets* 8: 583 – 602

Aronov S, Aranda G, Behar L, Ginzburg I (2001) Axonal tau mRNA localization coincides with tau protein in living neuronal cells and depends on axonal targeting signal. *J Neurosci* 21: 6577 – 6587

Artola A, von Frijtag JC, Fermont PC, Gispen WH, Schrama LH, Kamal A, Spruijt BM (2006) Long-lasting modulation of the induction of LTD and LTP in rat hippocampal CA1 by behavioural stress and environmental enrichment. *Eur J Neurosci* 23: 261 – 272

Attardo A, Fitzgerald JE, Schnitzer MJ (2015) Impermanence of dendritic spines in live adult CA1 hippocampus. *Nature* 523: 592 – 596

Avila J, Lucas JJ, Perez M, Hernandez F (2004) Role of tau protein in both physiological and pathological conditions. *Physiol Rev* 84: 361 – 384

Bai F, Bergeron M, Nelson DL (2003) Chronic AMPA receptor potentiator (LY451646) treatment increases cell proliferation in adult rat hippocampus. *Neuropharmacology* 44: 1013 – 1021

Ballatore C, Lee VM, Trojanowski JQ (2007) Tau-mediated neurodegeneration in Alzheimer's disease and related disorders. *Nat Rev Neurosci* 8: 663 – 672

de Barreda EG, Dawson HN, Vitek MP, Avila J (2010) Tau deficiency leads to the upregulation of BAF-57, a protein involved in neuron-specific gene repression. *FEBS Lett* 584: 2265 – 2270

Bullmann T, de Silva R, Holzer M, Mori H, Arendt T (2007) Expression of embryonic tau protein isoforms persist during adult neurogenesis in the hippocampus. *Hippocampus* 17: 98 – 102

Caceres A, Kosik KS (1990) Inhibition of neurite polarity by tau antisense oligonucleotides in primary cerebellar neurons. *Nature* 343: 461 – 463

Cheng JS, Craft R, Yu GQ, Ho K, Wang X, Mohan G, Mangnitsky S, Ponnusamy R, Mucke L (2014) Tau reduction diminishes spatial learning and memory deficits after mild repetitive traumatic brain injury in mice. *PLoS One* 9: e115765

Collingridge GL, Isaac JT, Wang YT (2004) Receptor trafficking and synaptic plasticity. *Nat Rev Neurosci* 5: 952 – 962

Dawson HN, Ferreira A, Eyster MV, Ghoshal N, Binder LI, Vitek MP (2001) Inhibition of neuronal maturation in primary hippocampal neurons from tau deficient mice. *J Cell Sci* 114: 1179 – 1187

Decker JM, Kruger L, Sydow A, Zhao S, Frotscher M, Mandelkow E, Mandelkow EM (2015) Pro-aggregant Tau impairs mossy fiber plasticity due to structural changes and Ca++ dysregulation. *Acta Neuropathol Commun* 3: 23

Detke MJ, Rickels M, Lucki I (1995) Active behaviors in the rat forced swimming test differentially produced by serotonergic and noradrenergic antidepressants. *Psychopharmacology* 121: 66 – 72

Frandemiche ML, De Seranno S, Rush T, Borel E, Elie A, Arnal I, Lante F, Buisson A (2014) Activity-dependent tau protein translocation to excitatory synapse is disrupted by exposure to amyloid-beta oligomers. *J Neurosci* 34: 6084 – 6097

Fuster-Matanzo A, de Barreda EG, Dawson HN, Vitek MP, Avila J, Hernandez F (2009) Function of tau protein in adult newborn neurons. *FEBS Lett* 583: 3063 – 3068

Garthe A, Behr J, Kempermann G (2009) Adult-generated hippocampal neurons allow the flexible use of spatially precise learning strategies. *PLoS One* 4: e5464

Goedert M, Spillantini MG, Jakes R, Rutherford D, Crowther RA (1989) Multiple isoforms of human microtubule-associated protein tau: sequences and localization in neurofibrillary tangles of Alzheimer's disease. *Neuron* 3: 519 – 526

Gould E, Cameron HA, Daniels DC, Woolley CS, McEwen BS (1992) Adrenal hormones suppress cell division in the adult rat dentate gyrus. *J Neurosci* 12: 3642 – 3650

Gould E, McEwen BS, Tanapat P, Galea LA, Fuchs E (1997) Neurogenesis in the dentate gyrus of the adult tree shrew is regulated by psychosocial stress and NMDA receptor activation. *J Neurosci* 17: 2492 – 2498

Groc L, Choquet D, Chaouloff F (2008) The stress hormone corticosterone conditions AMPAR surface trafficking and synaptic potentiation. *Nat Neurosci* 11: 868 – 870

Gu J, Firestein BL, Zheng JQ (2008) Microtubules in dendritic spine development. *J Neurosci* 28: 12120 – 12124

Harada A, Oguchi K, Okabe S, Kuno J, Terada S, Ohshima T, Sato-Yoshitake R, Takei Y, Noda T, Hirokawa N (1994) Altered microtubule organization in small-calibre axons of mice lacking tau protein. *Nature* 369: 488 – 491

Hernandez F, Avila J (2010) Intra- and extracellular protein interactions with tau. *Curr Alzheimer Res* 7: 670 – 676

Hirokawa N, Funakoshi T, Sato-Harada R, Kanai Y (1996) Selective stabilization of tau in axons and microtubule-associated protein 2C in cell bodies and dendrites contributes to polarized localization of cytoskeletal proteins in mature neurons. *J Cell Biol* 132: 667 – 679

Holth JK, Bomben VC, Reed JG, Inoue T, Younkin L, Younkin SG, Pautler RG, Botas J, Noebels JL (2013) Tau loss attenuates neuronal network hyperexcitability in mouse and Drosophila genetic models of epilepsy. *J Neurosci* 33: 1651 – 1659

Hu X, Viesselmann C, Nam S, Merriam E, Dent EW (2008) Activity-dependent dynamic microtubule invasion of dendritic spines. *J Neurosci* 28: 13094 – 13105

Hu YS, Long N, Pigino G, Brady ST, Lazarov O (2013) Molecular mechanisms of environmental enrichment: impairments in Akt/GSK3beta, neurotrophin-3 and CREB signaling. *PLoS One* 8: e64460

Ikegami S, Harada A, Hirokawa N (2000) Muscle weakness, hyperactivity, and impairment in fear conditioning in tau-deficient mice. *Neurosci Lett* 279: 129 – 132

Ittner LM, Ke YD, Delerue F, Bi M, Gladbach A, van Eersel J, Wolfing H, Chieng BC, Christie MJ, Napier IA, Eckert A, Staufenbiel M, Hardeman E, Gotz J (2010) Dendritic function of tau mediates amyloid-beta toxicity in Alzheimer's disease mouse models. *Cell* 142: 387 – 397

Jaworski J, Kapitein LC, Gouveia SM, Dortland BR, Wulf PS, Grigoriev I, Camera P, Spangler SA, Di Stefano P, Demmers J, Krugers H, Defilippi P, Akhmanova A, Hoogenraad CC (2009) Dynamic microtubules regulate dendritic spine morphology and synaptic plasticity. *Neuron* 61: 85 – 100

Kelsch W, Lin CW, Lois C (2008) Sequential development of synapses in dendritic domains during adult neurogenesis. *Proc Natl Acad Sci USA* 105: 16803 – 16808

Kempermann G, Kuhn HG, Gage FH (1997) More hippocampal neurons in adult mice living in an enriched environment. *Nature* 386: 493 – 495

Kimura T, Whitcomb DJ, Jo J, Regan P, Piers T, Heo S, Brown C, Hashikawa T, Murayama M, Seok H, Sotiropoulos I, Kim E, Collingridge GL, Takashima A, Cho K (2014) Microtubule-associated protein tau is essential for long-term depression in the hippocampus. *Philos Trans R Soc Lond B Biol Sci* 369: 20130144

Lei P, Ayton S, Moon S, Zhang Q, Volitakis I, Finkelstein DI, Bush AI (2014) Motor and cognitive deficits in aged tau knockout mice in two background strains. *Mol Neurodegener* 9: 29

Llorens-Martin M, Fuster-Matanzo A, Teixeira CM, Jurado-Arjona J, Ulloa F, Defelipe J, Rabano A, Hernandez F, Soriano E, Avila J (2013) GSK-3beta overexpression causes reversible alterations on postsynaptic densities and dendritic morphology of hippocampal granule neurons in vivo. *Mol Psychiatry* 18: 451 – 460

Llorens-Martin M, Jurado-Arjona J, Avila J, Hernandez F (2015) Novel connection between newborn granule neurons and the hippocampal CA2 field. *Exp Neurol* 263: 285 – 292

Llorens-Martin M, Lopez-Domenech G, Soriano E, Avila J (2011) GSK3beta is involved in the relief of mitochondria pausing in a Tau-dependent manner. *PLoS One* 6: e27686

Llorens-Martin M, Teixeira CM, Fuster-Matanzo A, Jurado-Arjona J, Borrell V, Soriano E, Avila J, Hernandez F (2012) Tau isoform with three microtubule binding domains is a marker of new axons generated from the subgranular zone in the hippocampal dentate gyrus: implications for Alzheimer's disease. *J Alzheimers Dis* 29: 921 – 930

Llorens-Martin M, Tejeda GS, Trejo JL (2010) Differential regulation of the variations induced by environmental richness in adult neurogenesis as a function of time: a dual birthdating analysis. *PLoS One* 5: e12188

Llorens-Martin M, Trejo JL (2011) Mifepristone prevents stress-induced apoptosis in newborn neurons and increases AMPA receptor expression in the dentate gyrus of C57/BL6 mice. *PLoS One* 6: e28376

Lu M, Kosik KS (2001) Competition for microtubule-binding with dual expression of tau missense and splice isoforms. *Mol Biol Cell* 12: 171 – 184

Lugert S, Basak O, Knuckles P, Haussler U, Fabel K, Gotz M, Haas CA, Kempermann G, Taylor V, Giachino C (2010) Quiescent and active hippocampal neural stem cells with distinct morphologies respond selectively to physiological and pathological stimuli and aging. *Cell Stem Cell* 6: 445 – 456

Ma QL, Zuo X, Yang F, Ubeda OJ, Gant DJ, Alaverdyan M, Kiosea NC, Nazari S, Chen PP, Nothias F, Chan P, Teng E, Frautschy SA, Cole GM (2014) Loss of MAP function leads to hippocampal synapse loss and deficits in the Morris Water Maze with aging. *J Neurosci* 34: 7124 – 7136

Maphis N, Xu G, Kokiko-Cochran ON, Cardona AE, Ransohoff RM, Lamb BT, Bhaskar K (2015) Loss of tau rescues inflammation-mediated neurodegeneration. *Front Neurosci* 9: 196

Ming GL, Song H (2005) Adult neurogenesis in the mammalian central nervous system. *Annu Rev Neurosci* 28: 223 – 250

Moghaddam B, Bolinao ML, Stein-Behrens B, Sapolsky R (1994) Glucocorticoids mediate the stress-induced extracellular accumulation of glutamate. *Brain Res* 655: 251 – 254

Mondragon-Rodriguez S, Trillaud-Doppia E, Dudilot A, Bourgeois C, Lauzon M, Leclerc N, Boehm J (2012) Interaction of endogenous tau protein with synaptic proteins is regulated by N-methyl-D-aspartate receptor-dependent tau phosphorylation. *J Biol Chem* 287: 32040 – 32053

Nair A, Bonneau RH (2006) Stress-induced elevation of glucocorticoids increases microglia proliferation through NMDA receptor activation. *J Neuroimmunol* 171: 72 – 85

Regan P, Piers T, Yi JH, Kim DH, Huh S, Park SJ, Ryu JH, Whitcomb DJ, Cho K (2015) Tau phosphorylation at serine 396 residue is required for Hippocampal LTD. *J Neurosci* 35: 4804 – 4812

Roberson ED, Halabisky B, Yoo JW, Yao J, Chin J, Yan F, Wu T, Hamto P, Devidze N, Yu GQ, Palop JJ, Noebels JL, Mucke L (2011) Amyloid-beta/

Fyn-induced synaptic, network, and cognitive impairments depend on tau levels in multiple mouse models of Alzheimer's disease. *J Neurosci* 31: 700 – 711

Roberson ED, Scearce-Levie K, Palop JJ, Yan F, Cheng IH, Wu T, Gerstein H, Yu GQ, Mucke L (2007) Reducing endogenous tau ameliorates amyloid beta-induced deficits in an Alzheimer's disease mouse model. *Science* 316: 750 – 754

Sahay A, Hen R (2008) Hippocampal neurogenesis and depression. *Novartis Found Symp* 289: 152 – 160; discussion 160–154, 193–155

Sapir T, Frotscher M, Levy T, Mandelkow EM, Reiner O (2012) Tau's role in the developing brain: implications for intellectual disability. *Hum Mol Genet* 21: 1681 – 1692

Sayas CL, Tortosa E, Bollati F, Ramirez-Rios S, Arnal I, Avila J (2015) Tau regulates the localization and function of End-binding proteins 1 and 3 in developing neuronal cells. *J Neurochem* 133: 653 – 667

Sokolow S, Henkins KM, Bilousova T, Gonzalez B, Vinters HV, Miller CA, Cornwell L, Poon WW, Gylys KH (2015) Pre-synaptic C-terminal truncated tau is released from cortical synapses in Alzheimer's disease. *J Neurochem* 133: 368 – 379

Song J, Sun J, Moss J, Wen Z, Sun GJ, Hsu D, Zhong C, Davoudi H, Christian KM, Toni N, Ming GL, Song H (2013) Parvalbumin interneurons mediate neuronal circuitry-neurogenesis coupling in the adult hippocampus. *Nat Neurosci* 16: 1728 – 1730

Toni N, Laplagne DA, Zhao C, Lombardi G, Ribak CE, Gage FH, Schinder AF (2008) Neurons born in the adult dentate gyrus form functional synapses with target cells. *Nat Neurosci* 11: 901 – 907

Toni N, Sultan S (2011) Synapse formation on adult-born hippocampal neurons. *Eur J Neurosci* 33: 1062 – 1068

Vossel KA, Zhang K, Brodbeck J, Daub AC, Sharma P, Finkbeiner S, Cui B, Mucke L (2010) Tau reduction prevents Abeta-induced defects in axonal transport. *Science* 330: 198

Waterhouse EG, An JJ, Orefice LL, Baydyuk M, Liao GY, Zheng K, Lu B, Xu B (2012) BDNF promotes differentiation and maturation of adult-born neurons through GABAergic transmission. *J Neurosci* 32: 14318 – 14330

Weingarten MD, Lockwood AH, Hwo SY, Kirschner MW (1975) A protein factor essential for microtubule assembly. *Proc Natl Acad Sci USA* 72: 1858 – 1862

Zhao C, Teng EM, Summers RG Jr, Ming GL, Gage FH (2006) Distinct morphological stages of dentate granule neuron maturation in the adult mouse hippocampus. *J Neurosci* 26: 3 – 11

